Available online at www.sciencedirect.com

ScienceDirect

Green Energy & Environment 10 (2025) 937−966

www.keaipublishing.com/gee

Review Article

Mechano-driven chemical reactions

Shaoxin Li [a,b], Jiajin Liu [a,b], Zhong Lin Wang [a,c,d,e,*], Di Wei [a,f,*]

[a] Beijing Institute of Nanoenergy and Nanosystems, Chinese Academy of Sciences, Beijing, 101400, China
[b] School of Nanoscience and Engineering, University of Chinese Academy of Sciences, Beijing, 100049, China
[c] Beijing Key Laboratory of Micro-Nano Energy and Sensor, Center for High-Entropy Energy and Systems, Beijing Institute of Nanoenergy and Nanosystems, Chinese Academy of Sciences, Beijing, 101400, China
[d] Guangzhou Institute of Blue Energy, Knowledge City, Huangpu District, Guangzhou, 510555, China
[e] Georgia Institute of Technology, Atlanta, GA, 30332-0245, USA
[f] Centre for Photonic Devices and Sensors, University of Cambridge, 9 JJ Thomson Avenue, Cambridge, CB3 0FA, UK

Received 11 June 2024; revised 12 July 2024; accepted 2 August 2024
Available online 8 August 2024

Abstract

Traditional chemical processes often generate substantial waste, leading to significant pollution of water, air, and soil. Developing eco-friendly chemical methods is crucial for economic and environmental sustainability. Mechano-driven chemistry, with its potential for material recyclability and minimal byproducts, is well-aligned with green chemistry principles. Despite its origins over 2000 years ago and nearly 200 years of scientific investigation, mechano-driven chemistry has not been widely implemented in practice. This is likely due to a lack of comprehensive understanding and the complex physical effects of mechanical forces, which challenge reaction efficiency and scalability. This review summarizes the historical development of mechano-driven chemistry and discusses its progress across various physical mechanisms, including mechanochemistry, tribochemistry, piezochemistry, and contact electrification (CE) chemistry. CE-induced chemical reactions, involving ion transfer, electron transfer, and radical generation, are detailed, emphasizing the dominant role of radicals initiated by electron transfer and the influence of ion transfer through electrical double layer (EDL) formation. Advancing efficient, eco-friendly, and controllable green chemical technologies can reduce reliance on traditional energy sources (such as electricity and heat) and toxic chemical reagents, fostering innovation in material synthesis, catalytic technologies, and establishing a new paradigm for broader chemical applications.

Keywords: Mechano-driven; Mechanochemistry; Tribochemistry; Piezochemistry; Contact electrification

1. Introduction

In nature, mechanical processes, physical phenomena, and chemical reactions are intricately intertwined, shaping myriad natural landscapes and intricate material transformations. It is widely acknowledged that mechanical forces possess the capacity to alter the physical state of substances, such as through shape deformation or structural transformation. More interestingly, a multitude of chemical phenomena are observed in, or closely related to, such physical and mechanical processes. For instance, the extreme pressure and temperature in the Earth's crust can change crystal structures, leading to the genesis of new minerals. Crustal movements subject rocks to forces including compression, torsion, and tension, precipitating deformation, rupture, and reorganization of chemical bonds, thereby creating rocks with diverse chemical properties and structures. Moreover, weathering and hydraulic forces exert mechanical pressures on rock surfaces, triggering erosion and the dislodgment of particles, profoundly influencing the chemical composition and structure of rocks. Phenomena such as muscle contractions and skeletal movements involve

* Corresponding authors.
E-mail addresses: zhong.wang@mse.gatech.edu (Z.L. Wang), dw344@cam.ac.uk (D. Wei).
Peer review under the responsibility of Editorial Board of Green Energy & Environment

https://doi.org/10.1016/j.gee.2024.08.001

mechanical forces within organisms that exert a discernible impact on the chemical composition and structure of biological molecules and cellular formations. Therefore, scientists recognized that chemical reactions occur naturally in response to various mechanical processes [1], and the reaction products had the potential to generate diverse molecules capable of supporting extremophilic microbes [2], thereby influencing the early evolution of life [3].

In scientific research, there is a lack of detailed historical information regarding the initiation and timeline of the first mechano-driven reactions. In 315 B. C., the philosopher-scientist Theophrastus wrote a book entitled "On Stones", which recorded that cinnabar (HgS) could be reduced to mercury (Hg^0) through the grinding process, which involved a copper vessel and a copper pestle filled with some vinegar (containing acetic acid) [4]. However, following this probable pioneering example of a mechano-driven reaction, scarcely any such record had been found over a long period. It was not until 1820 that Faraday described a "dry way" approach to reduce silver chloride by grinding it with zinc, iron, tin, and copper in a mortar [5,6]. This recorded approach hinted at the existence of knowledge regarding mechano-driven reactions, but its casual terminology suggested that it had not attracted significant research interest from researchers. Matthew Carey Lea, referred to as the father of mechanochemistry, conducted an incidental experiment linking mechanical action and chemical response in 1866. Specifically, he used a glass rod to apply pressure on a sensitized photographic plate, "drawing" a developable pattern with light [7]. Subsequently, he established the first systematic investigations on chemical reactions in large numbers of compounds induced by mechanical grinding, and distinguished them from commonly used thermochemical methods [8]. Additionally, another prominent mechanochemist, Walther Spring, conducted a salt metathesis reaction between barium sulfate and sodium carbonate through repeated compression and pulverization in 1883 [9]. Interestingly, in 1893, Ling and Baker synthesized halogen derivatives of quinhydrone by grinding the reactants with small amounts of liquid, such as water or light petroleum [10]. This method is now referred to as the "liquid-assisted grinding (LAG)" method for mechano-driven reactions. In 1919, the term ''mechanochemistry'' was officially coined in the ''Textbook of General Chemistry'' by Wilhelm Ostwald [11]. He classified mechanochemistry as a branch of chemistry along with thermochemistry, photochemistry, and electrochemistry. Almost a century later, the International Mechanochemistry Association (IMA) was established in 1984, and subsequently became an associate member of the International Union of Pure and Applied Chemistry (IUPAC) [12]. Gerard Heinicke formalized mechanochemistry as "the discipline relative to physical-chemical modifications of the solid produced by the action of mechanical factors" [13].

Mechano-driven chemistry represents a genuinely interdisciplinary domain, including physics, chemistry, materials science, and mechanical engineering. Moreover, the research methodologies within mechanochemistry have gradually expanded to study the distinct objectives. In addition to the initial grinding techniques (mortar and pestle), mechanical action processes could be carried out by non-manual methods, such as ball mills, ultrasonication, atomic force microscope (AFM) and other mechanical equipment [14]. The search for "green" catalysis extends beyond traditional thermocatalytic, electrocatalytic, and photocatalytic fields [15], with mechano-driven chemistry emerging as a reliable and reproducible approach to achieve this objective. This work succinctly summarized the developmental history of mechano-driven chemistry in Fig. 1a. With the rapid progress of scientific technology, numerous physical effects and factors were being considered to explain or distinguish various mechano-driven reactions under different conditions. Although there have been many excellent reviews of mechano-driven chemistry with typical examples [16–18], the underlying mechanisms of mechano-driven reactions remain elusive and their reactive efficiency is still limited in scalability in practical applications. This is mostly because of a lack of comprehensive understanding for mechano-driven reactions with intricate interplay of multiple physical and chemical phenomena.

Different from most reviews that primarily offer insights from their respective fields, this work transcends these limitations by conducting a comprehensive review based on typical mechanochemical methods (e.g., mechanical force, friction, piezoelectricity, and contact electrification (CE)). We aim to provide insight into recent developments through representative examples, focusing on their reaction mechanisms and proposing perspectives for future advancement. The mechanism of mechano-driven chemical reactions could be generally divided into four parts. (1) *Mechanochemistry* explores the impact of local mechanical energy or force on reactant molecules to induce chemical reactions. Mechanochemistry minimizes dependence on hazardous or explosive metal reagents commonly used in conventional solvothermal syntheses, promoting the exploration of cost-effective, highly stable metal-free alternatives for green chemistry [19]. (2) The phenomenon of material chemical transformation during mechanical friction and wear at the interface is categorized as *tribochemistry*. The tribochemical reactions affect both the break-in of the mechanical system and its long-term lifetime, which can be controlled and be used to protect against wear. (3) Some reactions induced by piezoelectric materials under mechanical pressure or stress belong to *piezochemistry*, which investigates the correlation between piezoelectric effects and chemical reactions. Piezochemistry holds significant potential in catalytic reactions, particularly in elucidating the underlying correlation between catalytic activity and piezo physics. (4) The CE effect has garnered widespread attention in the field of mechano-driven reactions due to its ubiquity in various mechanical movements and its lack of restriction by material selection. Reactions induced by CE are termed contact-electro-chemistry (*CE-Chemistry*), focusing on interfacial charge transfer and chemical reactions. CE-Chemistry is an emerging technology that producing reactive oxygen substance (ROS) under the mild mechanical conditions, is highly consistent with the principle of green chemistry.

This work significantly summarizes several common forms of mechano-driven chemistry from different physicochemical

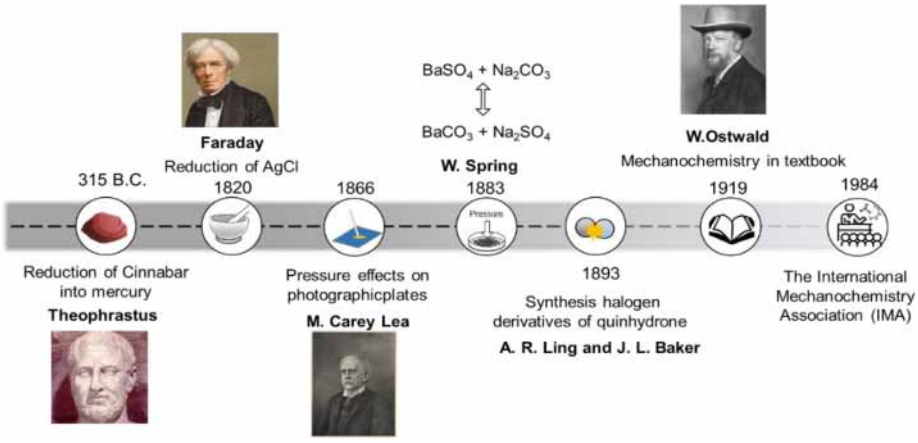

Fig. 1. The development of mechano-driven chemistry.

perspectives. Moreover, this work also elucidated the research focus and methods in different branches of mechano-driven chemistry, further reflecting the diversity and interdisciplinary nature of the field. Understanding mechano-driven reactions based on distinct mechanical and physical effects is beneficial for opening up effective and environmentally friendly avenues for new material synthesis, basic chemical research, and beyond. The work concluded with perspectives on current and near-term challenges for various branches of mechano-driven chemistry. It is acknowledged that while attempts have been made to summarize important and pertinent results, the vast amount of available literature renders it impossible to mention all references herein.

2. Methods of mechano-driven chemistry

Mechano-driven chemistry, which employs mechanical force to combine reactants and form products, is a truly interdisciplinary field encompassing physics, chemistry, materials science, and mechanical engineering. Typical methods and classifications of mechano-driven chemistry were shown in Fig. 2. Grinding reactants with a mortar and pestle is a straightforward method to form products without using liquid solutions or solvents. While this technique requires no specialized equipment and is feasible in any laboratory, it has limitations. It demands short reaction time for viability and often faces reproducibility challenges due to dependence on the operator's physical strength.

Ball milling is a more efficient grinding method performed by an instrument that grinds substances into a fine powder. The simplest ball mill consists of a cylindrical reaction vessel mounted on its side and spun around its central axis. The vessel is a jar filled with powdered chemical reactants and several hard balls. As a motor rotates the vessel, the balls roll up the vessel wall and then fall back onto the other balls in the chemical mixture. Each ball-on-ball strike crushes and mixes small amounts of powder at the strike point. This process continuously churns the materials through rotation and collision. Moreover, these instruments allow the energy input to be controlled by adjusting the milling frequency, thereby ensuring better reproducibility. Additionally, they are safer, as the reactions occur in closed vessels, protecting the operator from exposure to reactants, catalysts, and products. However, scaling this solvent-free chemical technology for commercial manufacturing remains a challenge.

Extrusion techniques have recently emerged as remarkably effective alternatives to milling, circumventing scalability and temperature control issues. Extrusion, commonly used in the polymer, materials, and food industries, is now being explored for continuous, scalable mechanochemical synthesis in fine-chemical production. In screw extruders (SE), solid reagents are ground together by a rotating screw while being transported along an extrusion path through a barrel. Different sections or zones of the screw can be exchanged to allow distinct mechanical actions (i.e., mixing, conveying, or grinding). The reagent feed rate, screw and barrel lengths, and screw-rotating speed can be adjusted to optimize reaction conditions. However, if the torque becomes too great, the screws can no longer turn, causing the reactor to automatically shut down. Additionally, a high reaction feed rate can lead to blockages, necessitating careful optimization of feed rates.

Although mechanochemistry can be readily conducted using ball-milling, extrusion, or other types of agitation, the mechanistic understanding of these processes remains limited due to substantial gaps in our comprehension of reaction kinetics. AFM and spectroscopy have represented a major advance in elucidating how directed mechanical force affects the structure and reactivity of molecules on surfaces, revealing how mechanochemistry can access unusual reaction products and selectivity.

In contrast to conventional mechano-driven chemical protocols, which typically require minimal solvent usage, mechanical and chemical effects promoted by ultrasound occur in a liquid medium. Ultrasonication can drive various reactions that usually happen only under extreme conditions through the cavitation effect. An oscillating bubble can accumulate energy from the ultrasonication in the form of heat. With continuing energy input, the bubble grows until reaching a size (typically tens of μm) at which the void structure is no longer stable. The bubble then suddenly collapses resulting in the rapid release of

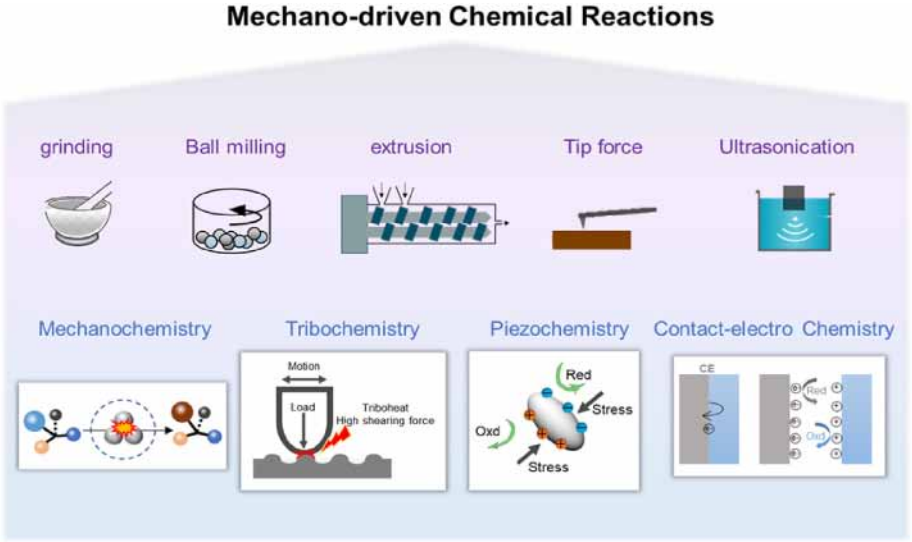

Fig. 2. Typical methods and classifications of mechano-driven chemistry.

the stored energy with a heating rate of $> 10^{10}$ K s^{-1}. This transient cavitation implosion is highly localized with associated temperature of roughly 5000 K and pressure of about 1000 bar. Ultrasonication offers several advantages, including low operating costs, simplicity of operation, modest power requirements, and the absence of a need for sophisticated equipment or intensive technical training. The diversity of mechanical methods suggests that mechano-driven chemical reactions exhibit various forms and working mechanisms. This review will detail several typical mechano-driven chemical reactions, including mechanochemistry, tribochemistry, piezochemistry, and CE-Chemistry.

3. Mechanochemistry

3.1. Mechanochemical reactions induced by different forces

Diverse phenomena in which mechanical load affects chemical reactivity were described by mechanochemistry. For instance, certain luminescent reactive molecules, known as mechanophores, undergo changes in intermolecular and intramolecular interactions under mechanical action [20], thereby altering the efficiency of fluorescence resonance energy transfer [21–24] or controlling excited-state intramolecular proton transfer [25]. These mechanophores are typically bound by weak covalent bonds [26]. When subjected to forces exceeding specific threshold values, they undergo homolytic or heterolytic cleavage [27–30], imparting mechanical color-changing responsiveness to polymers. This property is often utilized in pressure-sensing films, tamper-evident packaging materials, and early detection of structural damage [31–33]. Sagara et al. reported a supramolecular mechanical carrier based on cyclophanes, which exhibited reversible fluorescence upon deformation due to the elastic separation of quencher and emitter in space [34]. In cyclophane-based mechanical carriers, the intramolecular assembly of a blue-light emitting 1,6-bis(phenylethynyl)pyrene luminophore (blue) and a pyromellitic diimide (PMDI) quencher (brown) led to the formation of a charge-transfer (CT) complex (red) with reddish-orange emission (Fig. 3a(i)) [35]. Upon deformation of polyurethane (PU) elastomers containing the new mechanical carrier, the separation of the CT complexes resulted in an instantaneous, reversible and easily detectable emission color change (Fig. 3a(ii)). As shown in Fig. 3b, a linear, segmented PU elastomer covalently embedded with cyclophane 1 (1-PU) films exhibited orange fluorescence. Upon deformation, the color gradually shifted to blue, attributed to the reversible separation of the luminophore and quencher. In contrast, reference films did not show any detectable emission color change upon deformation. Regardless of the strain, a reference polymer containing compounds 2 (2-PU) and films of PU embedded with cyclophane 1 (1inPU) exhibited blue monomer emission and charge-transfer complex dominated orange emission, respectively. This new supramolecular cyclophane mechanophore, based on the change of emission species from CT-complex to monomer, allowed for the detection of mechanical events in polymers. It was useful for mechanistic studies, sensing applications, and failure detection. Polymers with force-induced luminescent properties could be employed to monitor and characterize the real-time response of materials to tensile or strain forces, revealing structural changes, chemical reactions, and energy release occurring within the material.

According to the classical theory of mechanochemistry, the shear deformation of solid reagents is accompanied by the formation of active states within the substance, the disordering of its structure, and the polarization of molecules [36–39]. Shear deformation provides numerous possibilities to overcome many processing obstacles typical for the interaction of hydrophilic polymers and hydrophobic organic reagents. Furthermore, mechanochemical synthesis, which involves the

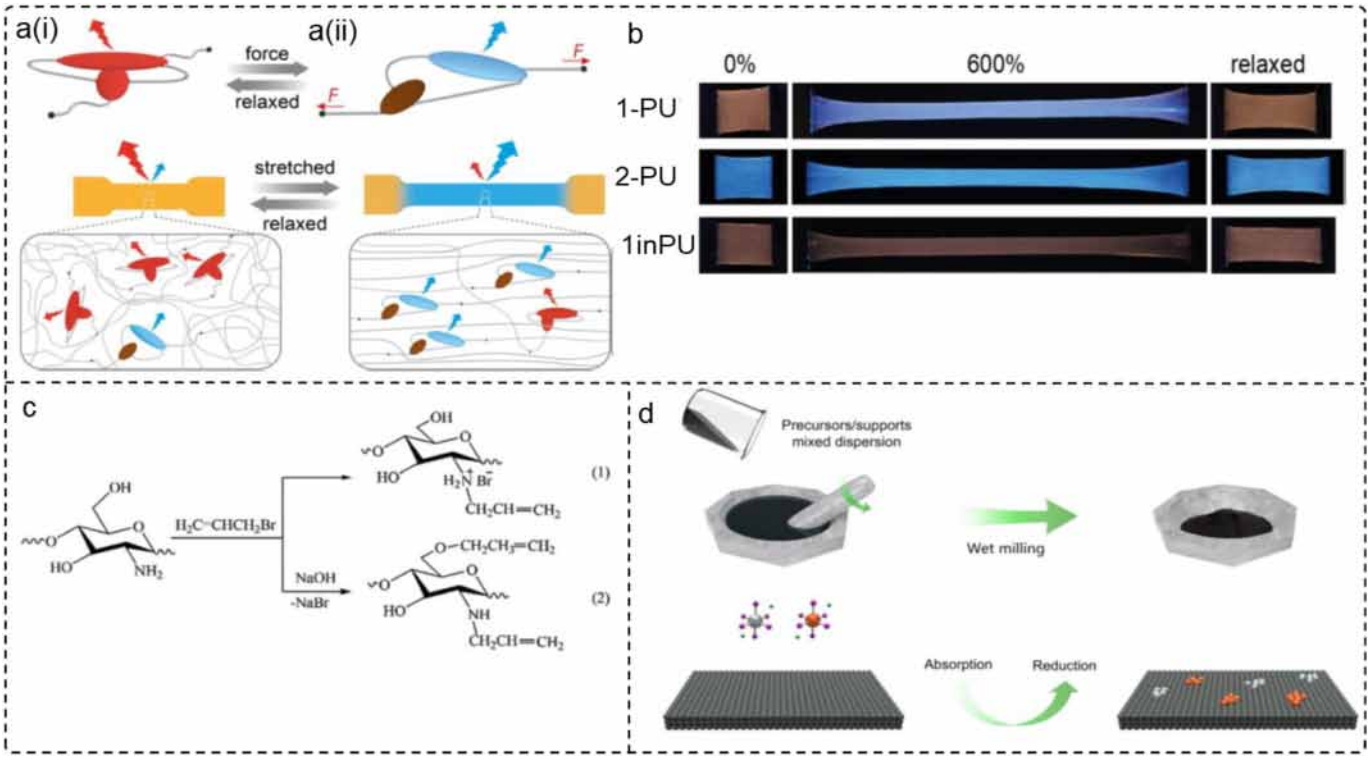

Fig. 3. **Mechanochemical reactions induced by different forces.** (a(i)) The cyclophane-based mechanophore and a(ii) its function in a polymer. Reprinted with permission from Ref. [35]. Copyright (2022) Clearance Center. (b) Pictures of 1-PU, 2-PU, and 1inPU films before stretching (left), strained to 600% (center), and after stress release (right). Reprinted with permission from Ref. [35]. Copyright (2022) Clearance Center. (c) Schemes of reactions occurred at solid-state synthesis in mixtures of chitosan and allyl bromide in the absence of NaOH (1) and alkaline medium (2). Reprinted with permission from Ref. [53]. Copyright (2019) Royal Society of Chemistry. (d) Schematic illustration of the wet milling synthesis process. Copyright (2022) Royal Society of Chemistry.

joint action of high pressure and shear strains on solid mixtures of reagents (including polymers) [14,40], can serve as an alternative method for producing polysaccharide derivatives. This method avoids the use of solvents and does not require the melting of reactive mixtures, making it a convenient and effective way of chemically modifying infusible polysaccharides. Due to the low thermal stability and long strain relaxation times of organic substances, particularly polymers, the most suitable technique for their solid-state modification is twin-screw extrusion. This method enables precise temperature control during the slow continuous deformation of solids [41,42]. As demonstrated by Akopova et al. highly deacetylated chitosan [43], its salts and complexes with bioactive organic compounds [44], as well as acylated and carboxymethylated derivatives could be produced via solid-state extrusion (Fig. 3c) [45,46]. A series of polysaccharide-based new materials have been obtained by co-extrusion of mixtures of polysaccharides such as chitosan, chitin, or cellulose with synthetic polymers or monomers [47–51]. Additionally, solvent-free synthesis of vinyl-substituted chitosan derivatives was achieved through co-extrusion of chitosan powder with allyl bromide under shear deformation [52]. This method indicated mechanochemistry can proceed without the need for any initiators and catalysts, making their products more simplicity and cleanliness with human health and the environment (simpler and cleaner for human health and the environment).

Some studies have also demonstrated that the use of an appropriate solvent could effectively enhance the efficiency of mechanochemical reactions. Du et al. reported a wet milling synthesis method to obtain Pt/Ir nanoclusters loaded on various substrates at room temperature [53]. Compared to traditional synthesis strategies [54–56], the wet milling synthesis method offers cost-effectiveness, environmental friendliness, and versatility. As shown in Fig. 3d, the ethanol solution of racemic Co_3O_4 and noble metal precursors was thoroughly stirred and transferred to an agate mortar. During wet milling, after the ethanol solvent evaporated in an open system, the resulting solution was directly converted into solid powder. Single-metal $Pt@Co_3O_4$ and $Ir@Co_3O_4$ catalysts were prepared using the same method as control samples. Compared to traditional solution-based synthesis methods that produce solid materials, the wet milling synthesis method eliminates the need for separating the product from the solvent and further purification processes. Importantly, incorporating appropriate volatile solvents in solid-state mechanochemical treatment allows for precise control over particle size, morphology, and uniformity. Due to its simplicity and versatility, this wet milling method is expected to further facilitate the large-scale preparation of supported noble metal catalysts and provide guidance for future endeavors in this field. It holds promising prospects for applications in various fields such as air purification, water treatment, industrial production, and renewable energy.

3.2. Mechanochemical reactions induced by ultrasonication

In structurally susceptible materials, polymers exhibit a wide range of mechano-driven reactions that can be controlled and amplified through mechanical force. Bielawski et al. inferred that the configuration inversion should proceed via a planar intermediate, which could be generated by tension exerted by polymer chains possessing a critical molecular weight on the naphthyl ring. This force ultimately overcame rotational constraints, thereby converting one enantiomer into another (Fig. 4a) [57]. Moreover, the mechanical activation of polymers appeared to depend largely on their molecular weight. Below a certain molecular weight threshold, the materials treated after ultrasonication showed no significant change compared to the pre-ultrasonicated polymers. In other words, polymer chains that were too short could not transmit the mechanical force required for bond breaking, although an increase in chain scission rate could be achieved when weak bonds existed at specific positions along the polymer backbone [38]. On the contrary, high molecular weight polymers were prone to degradation during ultrasonication. Chain scission along the polymer backbone occurred more rapidly than isomerization of the mechanical carriers, where selective bond cleavage at the chain center of the mechanical carrier was triggered by the mechanical force generated by ultrasonication. For instance, Sijbesma et al. applied this concept to activate catalysts that could further promote organic reactions [58]. Specifically, the metal center was chelated by two N-heterocyclic carbenes (NHCs), with each NHC connected to a polymer chain. Ultrasonication of longer polymers generated greater shear forces in the solution, ultimately breaking the metal–ligand bonds, resulting in active catalysts. Under ultrasonication, polymer-bound Agand Ru–NHCs catalyze ester exchanged reactions and ring-opening metathesis polymerization, respectively (Fig. 4b).

In recent years, the exploration of the coupling of mechanical force and bond breaking has promoted the development of mechanical responses in materials, such as damage sensing and self-strengthening. Lee et al. used sonochemical polymer mechanochemistry to assess the relative mechanical strength of a multicatenane copolymer relative to copolymers of cyclic and linear analogs (Fig. 4c(i)) [59]. The relative mechanical strengths were obtained by comparing the limiting molecular weights (M_{lim}) and contour lengths (L_{lim}) of the polymers under pulsed ultrasound of their dilute solutions. The values of M_{lim} and L_{lim}, and thus the inferred mechanical strengths of the polymers, were effectively identical (Fig. 4c(ii)). The mechanical bonds of the catenanes were therefore as strong, or stronger, mechanically as the covalent bonds along the polymer backbone. Additionally, to investigate the mechanochemical response of all block copolymers (BCPs), Zhang et al. prepared polymers containing different ratios of butyl acrylate and methyl methacrylate with similar degrees of polymerization (Fig. 4d(i)) and applied stress to them using ultrasonication [60]. Interestingly, BCPs, regardless of the amount of methyl methacrylate monomer, exhibited mechanochemical rate constants similar to those of methyl methacrylate homopolymers, while the response of random copolymers resembled that of acrylic ester homopolymers (Fig. 4d(ii)). Utilizing size exclusion chromatography coupled with multi-angle light scattering detection, the mechanochemical reaction corresponding to BCPs after ultrasonication treatment was carefully investigated. The results showed not only a shift in the main polymer peak to a longer retention time, which was common in homopolymers, but also the appearance of a new isolated peak with a retention time similar to that of the polymethyl methacrylate (PMMA) macroinitiator used to produce BCPs. (Fig. 4d(iii)). This observation suggested that C–C mechanochemistry occurred not only around the chain centers but also at the interfaces between blocks, resulting in the selective formation of distinct polymer peaks. Additionally, molecular dynamics modeling using acrylic acid ester and methyl methacrylate oligomers showed that dynamic phase separation occurred even in proper solvents, explaining the faster polymer mechanochemistry.

3.3. Mechanochemical reactions induced by ball milling

Ball milling procedures are one of the most important mechanochemical synthetic tools, since they can act as attractive alternatives to conventional grinding methods, such as grinding. Moreover, the advantages of ball milling methods include solvent-free reactions, faster reaction rates, and relatively pure products. Since Faraday's initial report on mechanochemical methods (also known as “dry way”) for conducting chemical reactions, the development of solvent-free ball milling or grinding methods in organic synthesis has sparked widespread theoretical and practical interest [12]. Additionally, under ball milling (solvent-free) conditions, the reaction medium evolves over time as the reagents and substrates gradually convert to the final products. In specific cases of organic/supramolecular/organometallic synthesis, ball milling or simple grinding had been shown to be more effective than reactions in solvents [61]. As shown in Fig. 5a, compared with conventional stirring methods, ball milling technology had been demonstrated to be a superior choice for asymmetric aldol reactions, resulting in shorter reaction times and higher stereoselectivity [62]. Although reactions took 48 h to complete with conventional magnetic stirring, they still proceeded with good yields. When the reaction was conducted in an organic solvent (such as tetrahydrofuran), racemic mixtures of the alcohol-aldehyde products were obtained after 10 days of reaction.

Mechanochemistry induced by ball milling can effectively facilitate the preparation of composite materials. Meng et al. proposed a solvent-free, green, and cost-effective preparation method using ball milling technology to fabricate functional epoxy resin/graphene nanocomposites [63]. During the ball milling process, graphene nanoplatelets (GnPs) were modified with long-chain surfactants, enabling better dispersion of graphene and establishing strong interfacial adhesion within the epoxy matrix, leading to significant improvements in functionality and mechanical properties (Fig. 5b). Compared to the

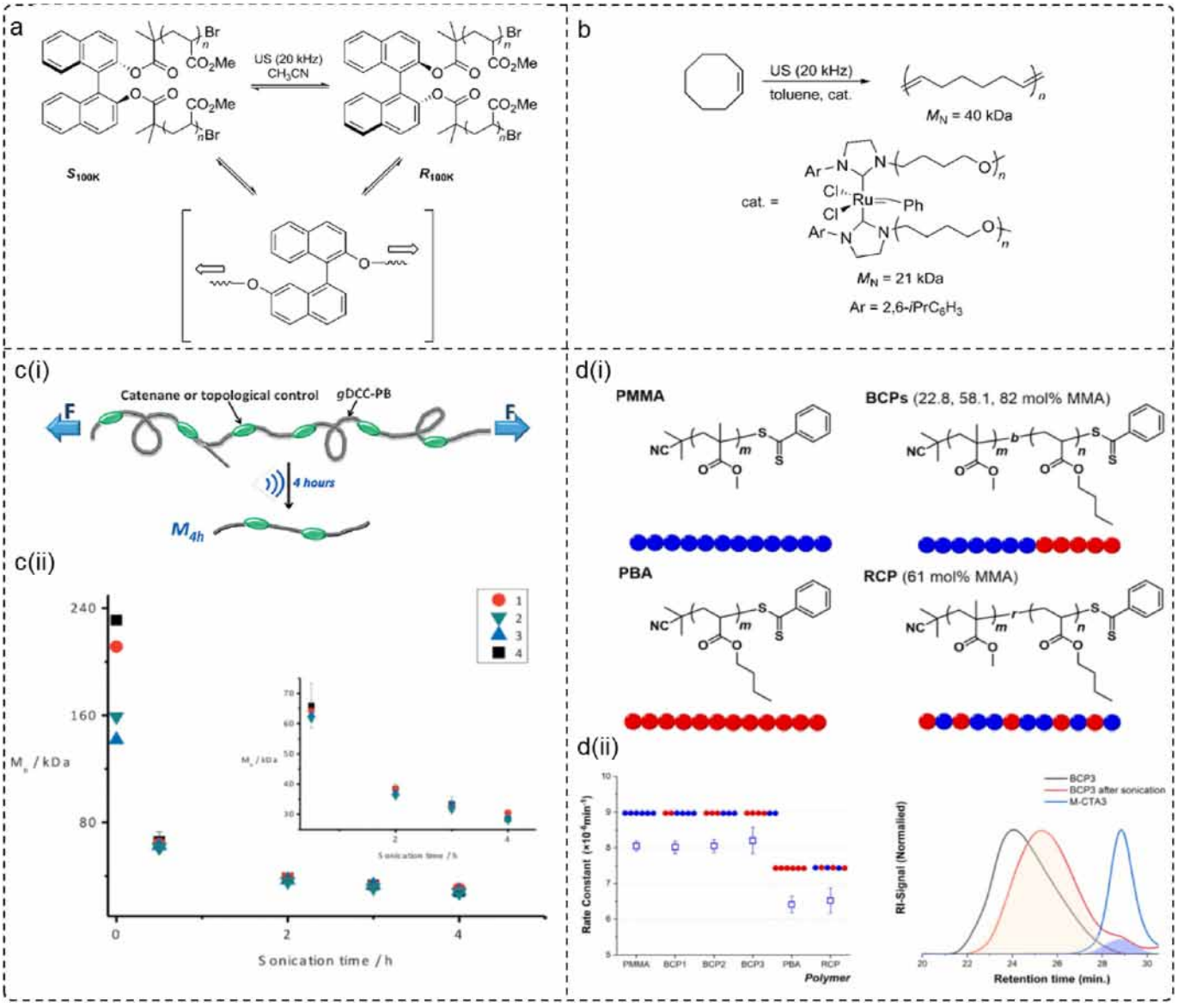

Fig. 4. **Mechanochemical reactions induced by ultrasonication.** (a) Configurational inversion of chiral atropisomers under ultrasonication. Reprinted with permission from Ref. [57]. Copyright (2010) by Copyright Clearance Center. (b) A catalytic mechanophore became active under ultrasonication only when the attached polymers reached a critical mass. Reprinted with permission from Ref. [57]. Copyright (2010) by Copyright Clearance Center. c(i) Schematic of strategy for characterizing the mechanical strength of mechanical bonds. c(ii) Decrease of molecular weight at time intervals during ultrasonication. After 4 h, the molecular weight of each polymer approaches between 28 and 30 kDa as M_{lim}. Reprinted with permission from Ref. [59]. Copyright (2016) by Copyright Clearance Center. d(i) Polymer structures of homopolymers, BCPs, and random copolymer. d(ii) Mechanochemical rate constants of the six polymers and SEC curves of BCP3 before and after ultrasonication, and the related macro-chain transfer agent. Reprinted with permission from Ref. [60]. Copyright (2023) by Copyright Clearance Center.

unmodified GnPs system, the modified GnPs (m-GnPs) exhibited enhanced dispersion quality and interfacial strength with the epoxy matrix, resulting in higher mechanical performance as well as improved electrical and thermal conductivity. This study demonstrated the tremendous potential of mechanochemical methods in the synthesis of functional epoxy resin/graphene composite materials. Moreover, Hao et al. investigated a Ni-catalyzed C–S coupling between bromides and disulfides under mild mechanochemical conditions. This study not only optimized the application of transition-metal catalyzed C–S coupling reactions but also advanced the development of an eco-friendly mechanochemical synthesis approach [15]. Additionally, Giri et al. utilized high-energy planetary milling to prepare polyethylene (PE)/iron composite materials [64]. Fang et al. synthesized ultrahigh molecular weight PE/hydroxyapatite composite materials through wet ball milling [65]. Planet mechanical milling was employed to successfully prepare UV-curable epoxy resin/organo-montmorillonite (OMMT) nanocomposites [66]. Deng et al. uniformly prepared UV-curable epoxy resin/OMMT nanocomposites using wet ball milling [67]. These advancements indicate that mechanochemistry is a rapidly evolving field in the preparation of composite materials.

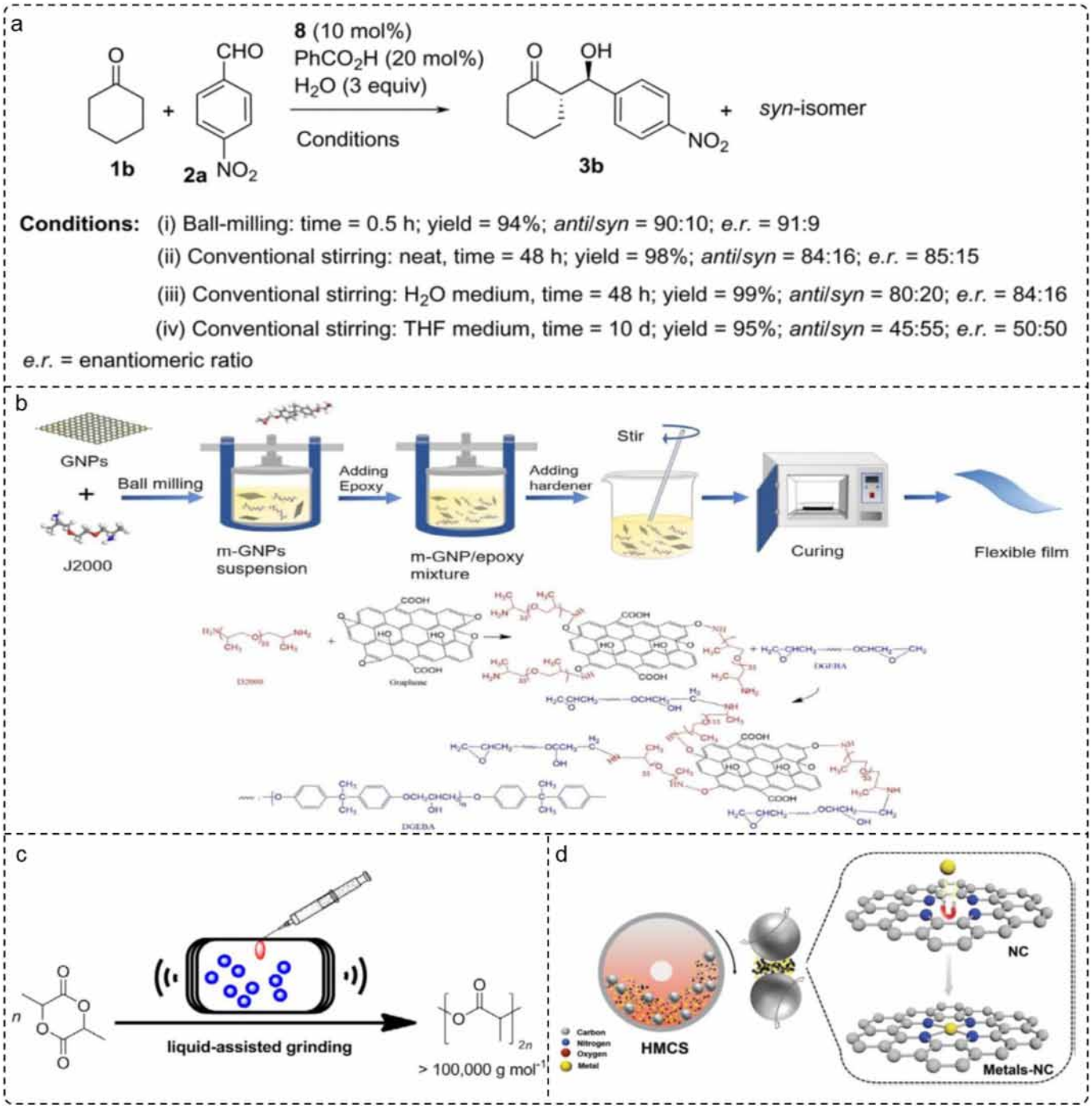

Fig. 5. **Mechanochemical reactions with ball milling.** (a) Comparative study employing ball milling and conventional magnetic stirring. Reprinted with permission from Ref. [62]. Copyright (2020) by Royal Society of Chemistry. (b) Illustration for preparation of m-GnP and reaction between GnPs and D2000. Reprinted with permission from Ref. [63]. Copyright (2016) by Copyright Clearance Center. (c) Mechanochemical ring-opening polymerization of lactide by ball milling. Reprinted with permission from Ref. [68]. Copyright (2016) by Copyright Clearance Center. (d) Illustration of the HMCS process. Reprinted with permission from Ref. [71]. Copyright (2016) by Copyright Clearance Center. Reprinted with permission from Ref. [93].

Ball milling process continuously agitates the materials through rotation and collision, enable precise control of energy input by adjusting the milling frequency, ensuring enhanced reproducibility. Moreover, they enhance safety by conducting reactions in closed vessels, shielding operators from exposure to reactants, catalysts, and products. Nevertheless, scaling this solvent-free chemical technology for commercial manufacturing presents ongoing challenges.

Liquid assisted grinding (LAG) is a common approach to accelerate or achieve mechanochemical solid-state reactions, in which a small amount of solvent (usually in drops) is used as an additive to enhance or control reactivity. Ohn et al.

conducted mechanochemical ring-opening polymerization of lactide using LAG technology [68,69]. Furthermore, the conversion of lactide to poly (lactic acid) was enhanced by LAG technology, compared to solvent-free ball milling. The degree of lactide ring-opening polymerization could be adjusted by ball milling time, vibration frequency, ball medium mass, and so on. While the chain scission of polymers induced by strong collision energy hindered the synthesis of high molecular weight polymers driven by mechanical force, the addition of a small amount of liquid enabled sufficient energy dissipation. Rissanen et al. utilized LAG to prepare halogen-bonded adducts and a halogen(I) complex akin to Barluenga's reagent, employing N-iodosaccharin. These mechanochemical materials were subsequently applied in the iodination of antipyrine, showcasing their promise as alternatives to Barluenga's reagent for both solution and solid-state synthesis, aligning with a modern, environmentally conscious approach [70]. In addition to synthesis reaction, LAG can create a better mixing environment between growing polymer chains and lactide monomers (Fig. 5c). This indicated that the use of LAG effectively prevented chain degradation during the polymerization process, ultimately producing poly (lactic acid) with molecular weights exceeding 100,000 g mol^{-1}.

Despite its feasibility and scalability, the mechanical energy applied in ball milling is largely arbitrary and difficult to quantify. To further advance mechanochemical synthesis, Liu et al. proposed a direct approach called heat mechanochemical synthesis (HMCS) to prepare special metal-nitrogen-doped carbonaceous (NC) materials (Fig. 5d) [71]. Specifically, the process entailed placing the NC matrix derived from the thermal decomposition of urea at elevated temperatures, alongside the requisite chemical additives and metal compounds, within an agate jar. Subsequently, subjecting it to ball milling at approximately 150 °C for a predetermined duration. Through thermal activation, the resultant material manifested augmented surface metal content and engendered distinctive metal sites amidst the collision of mechanical energy. Following robust acid leaching, and without necessitating high-temperature annealing, the material showed exceptional activity. This approach simultaneously provided mechanical energy and heat to drive the reaction, effectively encapsulating the target metal atoms within the pre-prepared nitrogen-doped and defect-rich carbon. Its merits include (1) enhanced metal content on the outermost surface; (2) generation of unique metal sites amid collisions of mechanical energy; (3) elimination of the requirement for high-temperature annealing, thereby preserving select active sites on the material. A suite of singly transition metal (e.g., Cr, Mn, Fe, Co, Ni, Cu, or Zn) surface-anchored carbons had been procured via the HMCS method. Furthermore, the facile one-step preparation of highly dispersed and anchored multiple metals (e.g., combinations thereof) on carbon materials was notably convenient.

4. Reactions induced by friction

With ongoing technological advancements, the field of mechano-driven reactions continues to expand. Mechanochemistry refers to reactions triggered by mechanical force, while those occurring at sliding interfaces are termed "tribochemistry." Unlike traditional mechanochemistry, tribochemistry reactions are primarily initiated at sliding interfaces due to friction and surface interactions. These interactions often lead to the formation of an intermediate layer, known as a "friction film", which serves to mitigate friction and wear [72]. The distinction between tribochemistry and mechanochemistry involves several factors [73], with the primary difference lying in the dissipation of energy. In tribochemistry, energy is primarily dissipated through shear at the interface of two surfaces, whereas mechanochemical processes, such as ball milling, initiate reactions by dissipating energy into the bulk material (Fig. 6a). Tribochemistry leverages externally applied work to influence the bond energies of materials, facilitating chemical bond rearrangement with reactants, and thereby reducing or replacing the activation energy associated with thermodynamics. The chemical rate kinetics of tribochemical reactions can be characterized by a reduction in activation energy with increasing externally applied stress, such as frictionally rubbing two interfaces together. Boldyrev demonstrated that shear stress, rather than normal stress, was the primary driving factor for film formation [74]. With advancements in computational power, enhanced modeling capabilities, and novel characterization methods, tribochemistry has emerged as a recognized interdisciplinary branch of chemistry.

In tribochemical reactions, various factors contribute significantly, among which frictional heat, wear, applied force, and frictional emission are particularly noteworthy. These elements co-occur during tribochemical reactions, lending a distinctive character to tribochemistry. Notably, surface wear during the reaction process emerges as a significant parameter warranting attention. Many material surfaces, especially metals and ceramics, possess highly oxidized boundary layers that act as barriers, separating the bulk material from oxygen-rich atmospheres and largely exhibiting chemical inertness. Early investigations underscored the importance of removing these outer layers through wear, thereby continuously exposing the fresh underlying material, which accelerates tribochemical reactions. Lubricant additives in tribochemical activation play a pivotal role by forming solid or viscous films, segregating surfaces within the boundary lubrication region. This action serves to prevent wear and mitigate friction, aligning with the objectives of tribochemical reactions [75]. The tribofilm formed during tribochemical reactions was initially discovered in zinc dialkyldithiophosphate (ZDDP) additives of lubricants [76], which improved the wear resistance of the lubricated surface [77]. Later, it was found that other additives could also form films with different friction behaviors through tribochemical reactions [78]. As shown in Fig. 6b(i), ZDDP was the first lubricant additive studied for tribochemical processes, highlighting the significance of friction conditions. From the late 1980s to the 1990s, new surface characterization methods greatly enhanced the understanding of the mechanisms behind tribochemical reactions. This also advanced the understanding of other tribochemically active

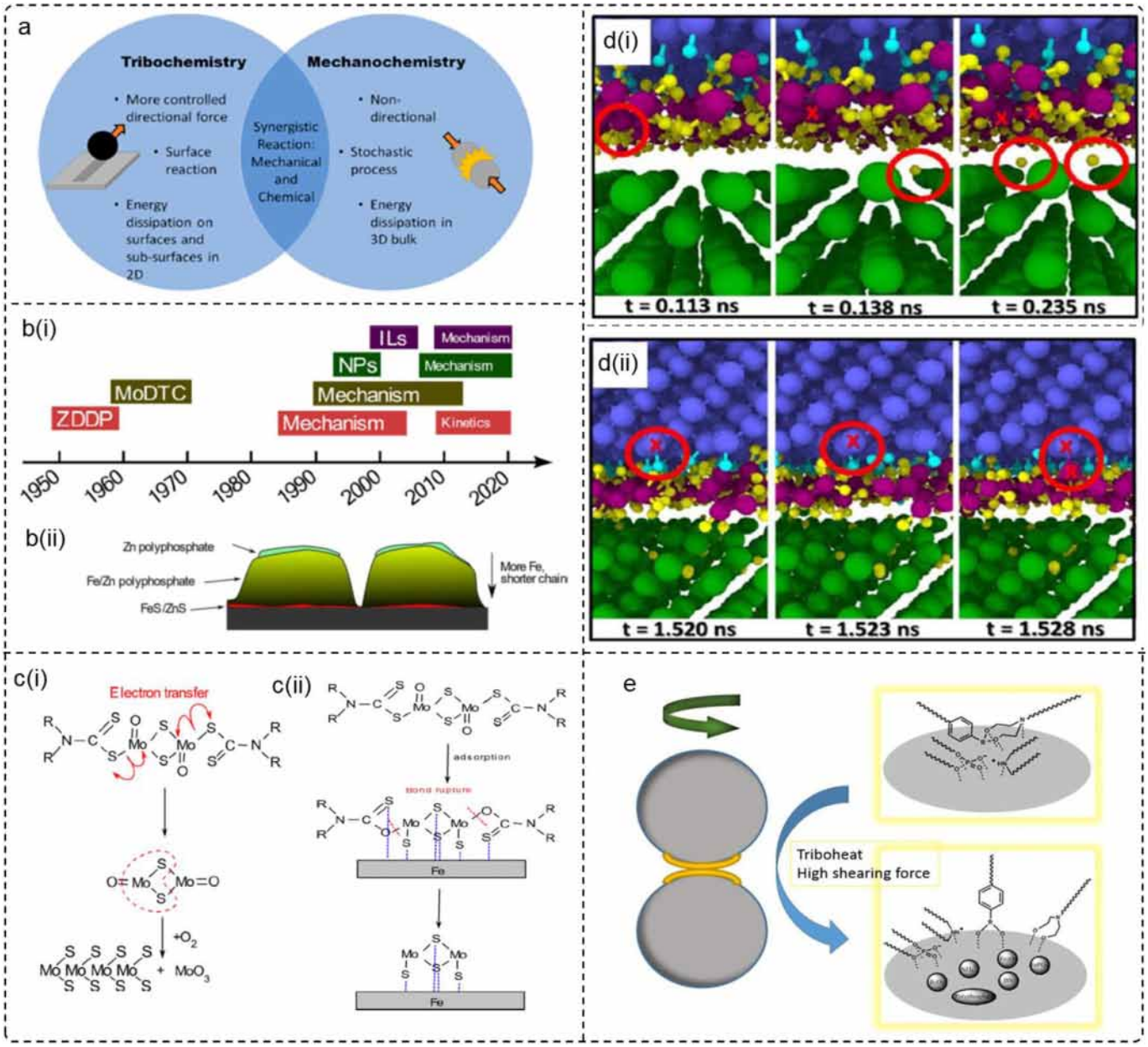

Fig. 6. **Reactions induced by friction.** (a) Direct comparison between tribochemistry and mechanochemistry. Reprinted with permission from Ref. [73]. Copyright (2020) by Creative Common CC BY. (b(i)) Development of tribochemically active lubricant additives, their reaction mechanisms, and underlying thermal dynamic principles. Reprinted with permission from Ref. [79]. Copyright (2020) by Creative Common. (b(ii)) Cross-section image of ZDDP tribofilms. Ref. [79]. Copyright (2020) by Creative Common. (c(i)) Mechanism of MoDTC tribochemical reaction by oxidation. Reprinted with permission from Ref. [79]. Copyright (2020) by Creative Common. (c(ii)) Mechanism of MoDTC tribochemical reaction by decomposing to LI. Reprinted with permission from Ref. [79]. Copyright (2020) by Creative Common. (d) Snapshots from reactive molecular dynamics simulations of hexadecane lubricated sliding of tungsten on diamond. Hexadecane lowers friction by physically separating the surfaces, as well as chemically by forming a low-density film on the surfaces. Reprinted with permission from Ref. [89]. Copyright (2020) by Creative Common. (e) A schematic diagram of the tribochemical reactions for the combination of DBDB and DOPD on the metal surface. Reprinted with permission from Ref. [93]. Copyright (2017) by Copyright Clearance Center.

lubricant additives, such as molybdenum dithiocarbamate (MoDTC) and molybdenum dithiophosphate (MoDTP). In the 2000s, the popularity of molecular dynamics methods further refined the elucidation of the mechanisms of tribochemical reactions.

Two novel types of lubricant additives, ionic liquids and nanoparticles, were developed over the past decade, with their reaction mechanisms elucidated after ten years of research. Fig. 6b(ii) illustrated the cross-section of the ZDDP friction film. Notably, friction films formed at lower temperatures exhibited longer polyphosphate chains [79], distinguishing them from thermal films that lack this oxide layer [80]. Moreover, the friction film exhibited better wear resistance than the thermal film [81]. Aktary et al. pointed out that the nano hardness of the ZDDP reaction film formed by tribochemical processes was twice that of the thermally formed

film [82]. Similar structures of molybdenum sulfide-based compounds were introduced in the 1970s, such as MoDTC and MoDTP. Unlike ZDDP, the friction films formed by MoDTC and MoDTP contained solid lubricant MoS_2 that could be as friction modifiers. However, the low shear strength of MoS_2 made the MoDTC and MoDTP friction films prone to wear [83]. This indicated that the low friction could not be maintained without continuous replenishment of MoDTC. Compared to ZDDP, MoDTC also exhibited a "fast" tribochemical reaction. When MoDTC was added to lubricating oil, the friction reduction effect was observed almost immediately [84]. In the late 1990s, Grossiord et al. proposed a route for the tribochemical decomposition of MoDTC [85]. Specifically, MoDTC on the friction surface first decomposed into two radicals, and the Mo radicals oxidized to form MoS_2 particles (Fig. 6c(i)). However, this pathway could not explain why MoDTC performs better when the metal oxide layer was stripped under vacuum [86]. Therefore, Onodera et al. proposed molecular dynamics simulations of the tribochemical reaction of MoDTC. They hypothesized that MoDTC initially formed a bridging isomer (LI-MoDTC, as depicted in Fig. 6c(ii)) due to its lower Gibbs free energy and the lower Gibbs free energy of the transition state compared to the intermediate Mo radical [87]. The simulation results indicated that these chemisorbed molecules would further decompose under frictional actions. The first bond to break was the Mo–O bond, which then directly formed MoS_2 along with the MoDTC. This molecular dynamic simulation pathway explained why MoDTC can undergo tribochemical reactions with a freshly exposed iron surface in a vacuum, as it does not require the presence of oxygen. Moreover, some researchers explored tribochemistry through "reactive" molecular dynamics simulations based on empirical models that capture chemical bond formation and breaking. These simulations had been employed to model interactions between lubricants and surfaces, providing insights into how lubricants function under various conditions. Recently, Romero et al. captured the sliding of hexadecane lubricated H-passivated diamond by simulation [88]. This study suggested that low friction was caused by a low-density hydrocarbon film formed by dehydrogenation of hexadecane lubricant molecules. As shown in Fig. 6d, the key step in the formation of this film was the transfer of hydrogen from hexadecane to the octahedral sites on the tungsten surface, followed by the chemical adsorption of hexadecyl radicals onto the dangling C-bond sites of the diamond [89]. As empirical potentials evolved to offer greater accuracy and became more accessible, and computational resources continued to advance in speed, reactive molecular dynamics simulations were poised to play a pivotal role in shaping novel concepts within tribological design.

In the past decade, ionic liquids had been reported as pure lubricants (or base oils) and lubricant additives, achieving promising results. Currently, they had sparked great interest in both fundamental and applied research fields. Ionic liquids are compounds consisting of asymmetric cations and anions. They manifest as liquids at temperatures below 100 °C, exhibiting negligible vapor pressure, elevated viscosity, non-flammability, strong affinity for metal ions, and exceptional thermal stability. These attributes are notable and modifiable, rendering them versatile in both their physical and chemical attributes [90,91]. Due to the unique geometric and charge properties of ionic liquids, the adsorption film of ionic liquids on metal surfaces can effectively act as a lubricant. On one hand, the irregular shapes of both cations and anions contribute to lower shear stress in comparison to non-polar molecular liquids, consequently resulting in reduced friction. On the other hand, the inherent polarity of ionic liquids facilitates frictional reactions when subjected to frictional heat and stress on the counterpart surface, consequently leading to the formation of boundary films [92]. Li et al. introduced the synergistic effect between phosphoric di(2-ethylhexyl) ammonium (DOPD) ionic liquid and 2-(4-dodecylphenyl)-6-octadecyl-1,3,6,2-dioxaborine (DBDB) in extreme pressure [93]. Their results indicated that DBDB and DOPD exhibited outstanding synergistic effects in extreme pressure, anti-friction, and anti-wear properties, which were enhanced with increasing external load. This excellent synergy arose from the effective collaboration of the friction reaction products generated by DBDB and DOPD, forming stable, dense, and low shear strength friction films. Firstly, the additive molecules adsorbed onto the metal surface to form an adsorption film (Fig. 6e). Then, the additives decompose, and the active elements participated in frictional chemical reactions, resulting in frictional chemical products composed of boric oxide (B_2O_3), boron nitride (BN), phosphates, and/or polyphosphates, organic amines, organic and/or inorganic amines, and iron oxide (Fe_2O_3). When the applied loads were above 196 N, more frictional heating and high shearing force as well as the mutual promotion between DBDB and DOPD led to the formation of a more compact and smooth protective film with low shearing strength, resulting in the low coefficient of friction of the combinations of DBDB and DOPD.

Furthermore, frictional heating at sliding interfaces plays a crucial role in driving tribological chemical reactions. The interaction between localized temperature and reaction rate is a well-established concept in chemistry based on the Arrhenius relationship [94]. In the field of tribochemistry, frictional heating refers to the localized temperature increase caused by sliding contact between two surfaces. In instances involving impeccably smooth surfaces, stress is uniformly dispersed across the complete contact area. Yet, in the realm of tangible surfaces characterized by inherent roughness, energy dissipates through the interaction of contact asperities. This contact typically leads to the generation of localized high temperatures, which exist for an extremely short duration. Due to the observation of flash temperatures at sliding contacts by Bowden et al. [95], surface temperature became a key factor for explaining almost all tribological chemical reactions by the latter half of the 1940s [96], along with some catalytic effects on the surface. Nevertheless, numerous tribochemical reactions defy simple explanation solely through surface temperature dynamics. They entailed a spectrum of dynamic physical processes underpinning friction, occurring both at and in proximity to the sliding contact interface.

Consequently, these reactions transcend traditional static reaction mechanisms reliant on heat and catalysis. Fig. 7a depicted schematic diagrams of three positions of frictional physical and tribochemical phenomena based on a frictional electromagnetic phenomenon model proposed by Nakayama et al. [97] As shown in Fig. 7a, the tribochemical reactions occurred within the in-contact area (ICA triboreactions), the near-contact area (NCA triboreactions) primarily consisted of the contact gap, and the outer contact area (OCA triboreactions) included worn surfaces away from the contact point. According to the location and frictional system, ICA reactions involved acid-base reactions and changes in crystal structure, while NCA reactions could be facilitated by electrons, ions, radicals, and photons generated in the frictional plasma to decompose adsorbed lubricants. In comparison to those high-energy processes, the action of OCA reactions was usually limited because of the lower number of low-energy electrons and the fewer surface species produced by static interactions. It is well known that the different reactions occur in various surface/interface regions. More importantly, the surface/interface region can also affect the reaction rate. Mori et al. delved into the decomposition of formic acid (HCOOH → H_2 + CO_2) during the scraping process [98]. They found that the adsorption of HCOOH was slow, while the desorption of

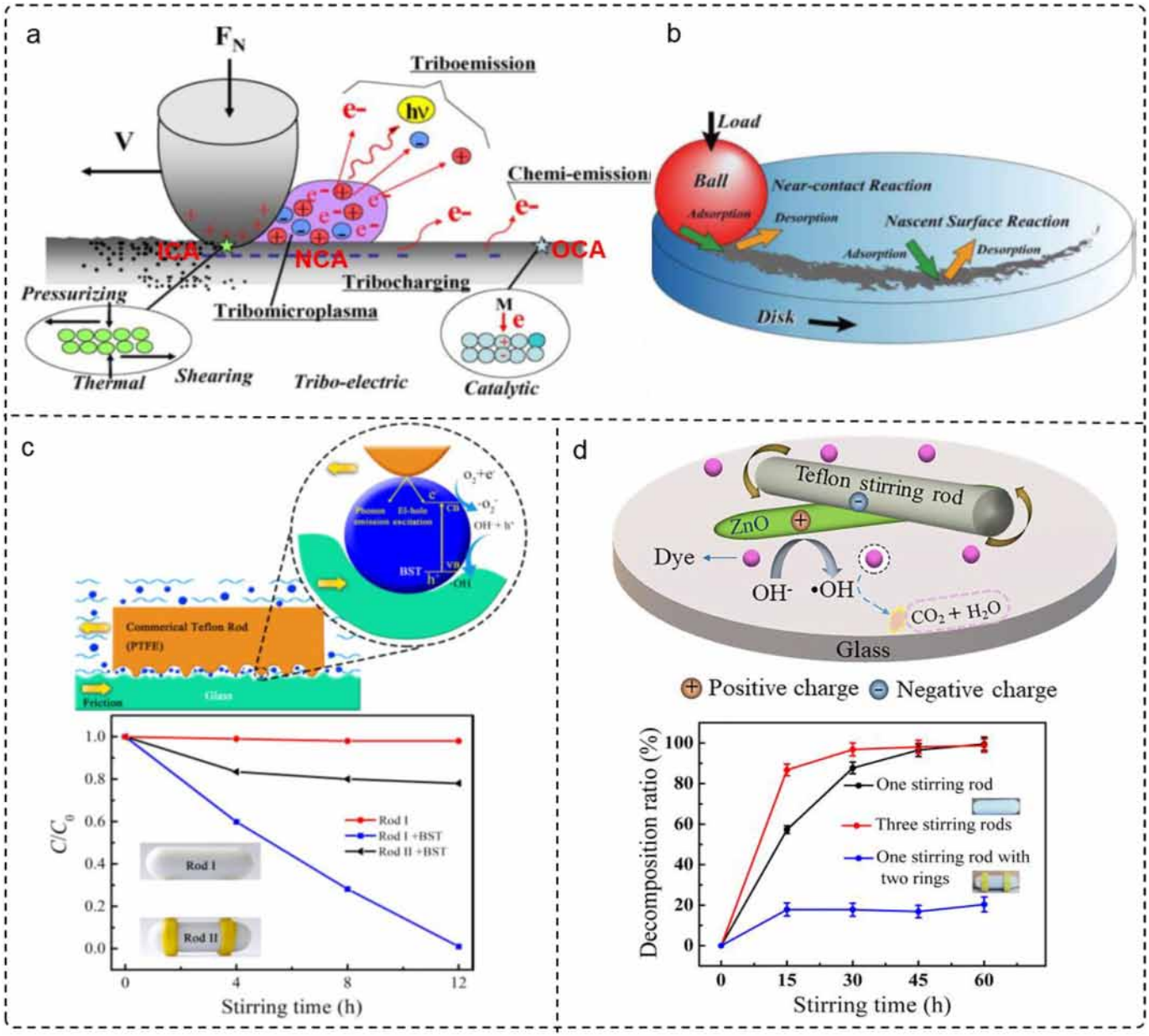

Fig. 7. **Tribochemistry.** (a) Conceptual view of tribochemical reactions at different positions of the contact zone. Reprinted with permission from Ref. [93]. Copyright (2017) by Copyright Clearance Center. (b) Two reaction areas that are responsible for quick and slow reactions. Reprinted with permission from Ref. [99]. Copyright (2017) by SAGE Publications Ltd. (c) The dye decomposition efficiency for RhB dye under magnetic stirring in dark at room temperature with different conditions. Ref. [100]. Copyright (2017) by Copyright Clearance Center. (d) The possible schematic diagram for the tribo–catalytic activity of ZnO nanorods, and the effect of amounts and types of stirring rods on the decomposition ratio. Reprinted with permission from Ref. [101]. Rightslink® by Copyright Clearance Center.

H_2 and CO_2 was fast. Their conclusion was that adsorption and desorption occurred at two separate sites on the freshly exposed surface. These two reactions should be assigned to different reaction regions, as shown in Fig. 7b [99]. Initially, a rapid reaction was initiated during the friction and wear process near the contact zone, characterized by the liberation of CO_2 and H_2. Subsequently, a gradual reaction ensued, linked to the formation of a freshly generated surface, precipitating water. The adsorption of gases occurred either proximate to the contact area or on the recently exposed surface post-contact, contingent upon the reaction mechanism. The disparity in time constants governing fast and slow reactions hinged upon the mode of reactant species supply. In the case of the slow reaction, the rate-determining step entailed either gas adsorption from the ambient environment or diffusion from the bulk. Conversely, for the fast reaction, the reactive gas was already prepped on the surface, poised for immediate reaction. The extent of the reaction was dictated by the frictional and wear processes dictating the interaction of the reactive gas on the catalyst surface.

Friction catalysis as a branch of tribology that studied changes in solid catalytic performance due to the influence of mechanical energy. The distinction between catalytic reactions and chemical reactions lies in the presence of a catalyst. The correlation between tribological chemistry and friction catalysis mirrors that of chemical and catalytic reactions. In essence, a chemical reaction intensified by friction in the absence of a catalyst is denoted as a tribochemical reaction, whereas with the presence of a catalyst, it transforms into a friction catalytic reaction. With frictional energy harvesting, Li et al. noted the spontaneous occurrence of dye decomposition in a suspension of $Ba_{0.75}Sr_{0.25}TiO_3$ (BST) nanoparticles (size: 20 nm) under normal stirring conditions in the absence of light at ambient temperature. (Fig. 7c) [100]. Crucially, they discovered that substantial improvements in decomposition efficiency could be attained through straightforward alterations to the stirring rod. This led to the decomposition of as much as 99.0% of Rhodamine B (RhB) within a span of 3 h, under mild stirring conditions at 300 r min^{-1}. Moreover, the dye decomposition was directly correlated with the friction between BST nanoparticles and the stirring rod during stirring process. It was believed that mechanical energy absorbed through friction enables BST nanoparticles to catalyze dye decomposition in a frictional catalytic process, as confirmed by the detection of intermediate species hydroxyl radicals ($\cdot OH$) and superoxide radical ($\cdot O_2^-$) during stirring. In addition, Zhao et al. discovered that hydrothermally synthesized zinc oxide (ZnO) nanorods exhibited excellent friction-catalyzed dye decomposition performance by harnessing the frictional energy generated during stirring (Fig. 7d) [101]. After stirring for 60 h, the friction-catalyzed dye decomposition rate reached approximately 99.8%. The advantages of ZnO nanorods with high dye decomposition rates hold potential for the treatment of dye wastewater using frictional energy available in the environment. These findings unmistakably showcased the capability of nanostructured oxide materials to utilize mechanical energy from their ambient surroundings, catalyzing dye decomposition through friction.

5. Reactions induced by piezoelectric effect

5.1. Band theory in piezochemistry

In 2010, Hong et al. discovered that the use of ultrasonic vibration of ZnO microfibers directly enabled water splitting and successful generation of H_2 and oxygen (O_2) (Fig. 8a) [102]. This finding linked the piezoelectric effect, which has been known for over 100 years, with chemical energy. The study demonstrated that under ultrasonic oscillation conditions in aqueous environments, the hexagonal structure of ZnO materials generated a non-zero dipole moment in the lattice, resulting in strain-induced surface charges. These charges could induce reduction and oxidation reactions by transferring to substances such as surface-adsorbed water molecules. The generated potential must exceed the standard redox potential of water (1.23 eV) to initiate redox reactions; otherwise, no reaction will occur. This research provided a simple and cost-effective direct water splitting technology that could generate hydrogen fuel by harnessing energy waste such as noise or stray vibrations in the environment. In recent decades, piezochemistry has emerged as a focal point of research, exploring the intricate interplay between mechano-driven piezoelectric effects and chemical reactions. Leveraging the distinctive attributes of piezoelectric materials, it aims to propel and regulate chemical transformations. Unraveling the underlying principles of piezoelectricity holds significant potential for advancing interdisciplinary. Drawing inspiration from photocatalysis, the band theory elucidates the behavior of piezoelectric materials in piezoelectric chemistry, delineating band levels comprising valence band (VB) and conduction band (CB). According to this theory, the piezoelectric potential induced within these materials by mechanical stress primarily functions as a “gate” to initiate chemical reactions. By fine-tuning the band structure and orchestrating the migration of internal charge carriers towards the material's surface, conducive conditions for reactions are established (Fig. 8b) [103]. Through the application of mechanical milling or ultrasonication, piezochemistry offers a promising avenue for the development of innovative synthesis routes, catalytic processes, and energy conversion technologies. Jiang et al. employed a unique $Bi_{25}FeO_{40}$ photochemical etching strategy to prepare $Bi_{25}FeO_{40}/Bi_2O_2CO_3$ (BFO/BCO) piezoelectric catalysts [104]. As a lead-free piezoelectric catalyst, the BFO/BCO piezoelectric composite material exhibited excellent degradation activity for 4-chlorophenol (4-CP) under ultrasonic vibration, with degradation efficiency exceeding 90% within 120 min. Introducing BCO onto through the action of the built-in electric field. It was also found that $\cdot OH$ and $\cdot O_2^- \cdot$ are the main active species responsible for the degradation of 4-CP. As shown in Fig. 8c (i), the piezoelectric catalytic performance of the composite material slightly decreased when potassium dichromate or sodium oxalate was added.

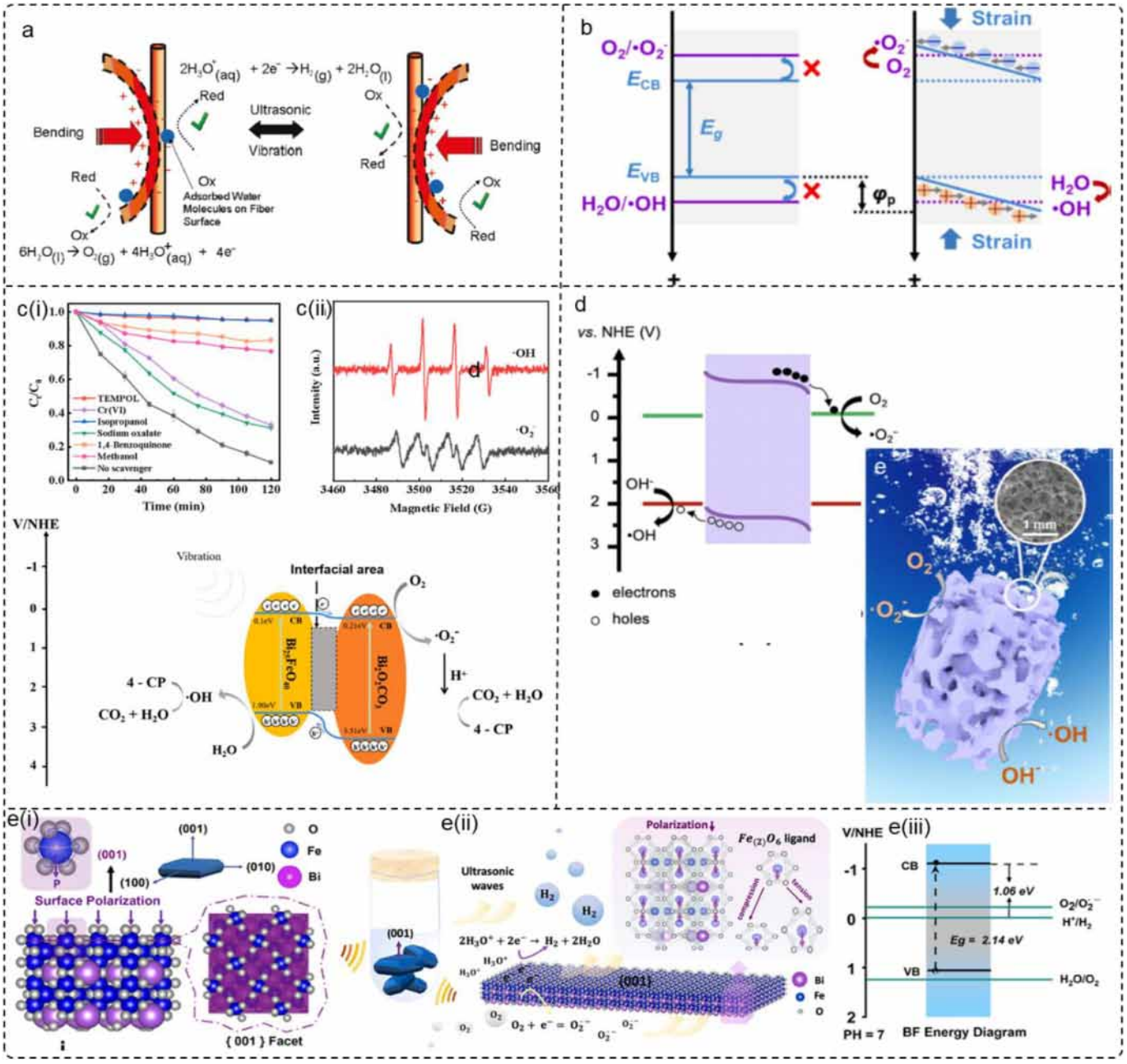

Fig. 8. **Band theory in piezochemistry.** (a) H_2 and O_2 were produced by deforming a ZnO fiber or $BaTiO_3$ dendrite inwater via redox reactions. Reprinted with permission from Ref. [102]. Rightslink® by American Chemical Society. (b) Schematic illustration of the energy band theory of piezocatalytic mechanism using the redox reactions of $O_2 + e \rightarrow \cdot O_2$ and $H_2O + h^+ \rightarrow \cdot OH + H^+$, where ECB and EVB were the positions of CB and VB, respectively, E_g and ϕ_P were energy band gap and piezopotential, respectively. Reprinted with permission from Ref. [103]. Rightslink® by Creative Commons CC-BY. (c(i)) Piezoelectric degradation curves of 4-CP by BFO/BOC with different trapping agents. (c(ii)) ESR spectra of BFO/BOC during the piezoelectric processes. (c(iii)) Piezoelectric catalytic mechanism of 4-CP by BFO/BOC. Reprinted with permission from Ref. [104]. Rightslink® by Copyright Clearance Center. (d) Schematic of porous piezocatalysis process in BTO-PDMS. Reprinted with permission from Ref. [107]. Rightslink® by American Chemical Society. (e(i)) Lattice distribution of BF nanoplates along (001), including details of $Fe_{(2)}O_6$ octahedral distortion and surface polarization. (e(ii)) A schematic illustration of the piezocatalytic mechanism during ultrasonic vibration. (e(iii)) An estimation of the energy band diagram of synthesized BF nanoplates with water splitting and superoxide redox potential vs. NHE. Reprinted with permission from Ref. [108]. Rightslink® by Copyright Clearance Center.

Moreover, the introduction of isopropanol, methanol, TEMPOL, and 1,4-benzoquinone significantly inhibited the piezoelectric catalytic performance, which capture e^-, h^+, $\cdot OH$, and $\cdot O_2^-$, respectively. Furthermore, the identification of sextet and quartet peaks via electron spin resonance (ESR) provided additional insight into the formation of $\cdot O_2^-$ and $\cdot OH$ radicals during the experimental procedure (Fig. 8c (ii)). Subsequently, the investigation proposed a mechanistic explanation for the augmented piezoelectric activity was observed in BFO/BOC composite materials. As illustrated in Fig. 8c (iii), the CB and VB of BFO were positioned at 0.1 eV and 1.9 eV, respectively, while those of BOC were situated at 0.21 eV and 3.51 eV

[105]. Due to the lower CB of BFO (0.1 eV) compared to that of BOC (0.21 eV), electrons from the CB of BFO could easily transfer to the CB of BOC. Simultaneously, owing to the higher VB of BOC (3.51 eV) compared to that of BFO (1.90 eV), holes from the VB of BOC could be injected into the VB of BFO. The heterojunction structure formed at the interface region between BFO and BOC generated an internal electric field, thereby facilitating the separation of electrons and holes. In the absence of externally applied ultrasound to induce piezoelectric polarization, charge carriers in the BFO/BOC composite material might migrate to either side. However, when ultrasound was applied to induce piezoelectric polarization, either BFO or BOC in the complex would undergo electron and hole separation in the direction opposite to polarization, and then electrons and holes participated in redox processes [106].

During the piezoelectric catalytic process, the introduction of micro-nano catalysts into water pollutants can lead to secondary contamination. Moreover, additional time and resources are required for recovery, measurement, and deposition or filtration procedures involving micrometer/nanometer particles. Qian et al. encapsulated piezoelectric particles in porous foam using polydimethylsiloxane (PDMS), as illustrated in Fig. 8d, presenting a facilely deployable and replaceable barium titanate ($BaTiO_3$) PDMS composite porous foam catalyst [107]. This design showcased advantages in recyclability and reusability, mitigating secondary pollution and enhancing repeatability thresholds. Under ultrasonic vibration, the piezoelectric $BaTiO_3$ material generated distinct electron–hole pairs, which subsequently reacted with hydroxide ions and oxygen molecules to yield $\cdot O_2^-$ and $\cdot OH$ radicals. Consequently, these radicals effectively degraded RhB dye solution by approximately 94%, with the composite material demonstrating exceptional stability after 12 cycles of repeated decomposition. The degradation efficiency of RhB was correlated with the piezoelectric constant, specific surface area, and morphology of the material. The piezoelectric material-PDMS composite porous foam catalyst for piezoelectric catalytic dye degradation presented promising prospects for future practical environmental purification applications.

In addition to conventional non-centrosymmetric piezoelectric materials characterized by remarkable piezoelectric coefficients, piezochemistry can also be realized using nanomaterials with centrosymmetric structures. The nanosheets of $Bi_2Fe_4O_9$ with a centrosymmetric structure were found to exhibit unprecedented high-pressure catalytic performance during the hydrogen evolution process (1058 μmol g^{-1} h^{-1} in pure water, 5723 μmol g^{-1} h^{-1} in 10% methanol) and organic degradation. Du et al. proposed a new perspective to elucidate the observed piezoelectric catalysis [108], suggesting that this piezoelectric property might originate from the presence of localized dipoles on exposed surfaces, which in turn arose from non-centrosymmetric ligands within the crystal cell. When external force was applied to the material, deformation caused by compressive or tensile stress altered the state of the dipole moment, originating from the non-centrosymmetric ligands exposed on the material surface, such as the $Fe_{(2)}O_6$ octahedra shown in Fig. 8e(i). Material deformation disrupted the charge balance in localized regions, thereby generating instantaneous electric fields that drove electron movement. The escaping electrons participated in redox reactions with hydrated hydrogen ions to produce hydrogen gas and reacted with oxygen to form superoxide, which was utilized for organic degradation (Fig. 8e(ii)). These surface polar structures provided functionality similar to spontaneous polarization in typical ferroelectric materials and did not form multi-domain structures due to oriented growth and precise arrangement of crystal cells in the single crystal. This naturally occurring surface polarization facilitated electron movement and mitigated carrier recombination, contributing to the excellent catalytic performance of $Bi_2Fe_4O_9$ nanosheets. Fig. 8e(iii) schematically illustrated the principle of the catalyst's band levels acting as gates to trigger redox reactions. The CB level of −1.06 eV (vs. NHE) was far more negative than the hydrogen reduction potential, substantiating the catalytic capacity of as-synthesized $Bi_2Fe_4O_9$ nanoplates for hydrogen evolution. Electrons in excited states were also capable of triggering the formation of $\cdot O_2^-$, which well explained the observed competence of BF nanoplates in RhB dye degradation.

5.2. Screening charge effect in piezochemistry

As indicated by band theory, the piezoelectric potential primarily serves as a “gate” to initiate reactions by modulating the band structure and regulating the movement of internal charge carriers toward the catalyst surface, facilitating reactions. In contrast, another mechanism, known as the screening charge effect, underscores the predominant influence of the piezoelectric potential and its related surface shielding behavior in piezoelectric materials [109]. The magnitude of the piezoelectric potential must accurately correspond to the required redox levels. It is crucial to ensure that the piezoelectric potential, serving as a driving force, fully meets or exceeds the specific Gibbs free energy change required for a given reaction, which is essential for piezoelectric catalysis. Moreover, the surface shielding behavior induced by polarization governs the piezoelectric catalysis process. Hence, a distinguishing characteristic between the screening charge effect and band theory is that the charges involved in the redox reactions originate from surface-adsorbed shielding charges from external systems, rather than from internal charges of the material.

Wang et al. reported a non-destructive, harmless, and convenient teeth whitening strategy based on the piezoelectric catalytic effect, achieved by replacing abrasive agents traditionally used in toothpaste with piezoelectric particles (Fig. 9a) [110]. Organic dyes were degraded by the piezoelectric catalysis of $BaTiO_3$ nanoparticles under ultrasonic vibration to simulate daily brushing. Teeth stained with tea, blueberry juice, wine, or their combinations were significantly whitened after 3 h of vibration with polarized $BaTiO_3$ turbid solution. Similar treatments using non-polarized or cubic $BaTiO_3$ showed negligible teeth-whitening effects. Moreover, the piezoelectric catalytic teeth whitening procedure based on

$BaTiO_3$ nanoparticles significantly reduced damage to tooth enamel and biological cells. Based on the generation of reactive oxygen species (ROS), such as ·OH and $\cdot O_2^-$, using $BaTiO_3$, the screening charge model of the piezoelectric catalytic process was demonstrated. In the pristine state (Fig. 9b(i)), surface-bound charges balance through screening charges to ensure the neutral electrostatic state of material [103]. During the application of external mechanical stress, the concentration of bound charges would change, and the associated movement of screening charges would occur on the surface. Charges can depart from the surface and reacted with localized substances such as water to produce ROS (Fig. 9b(ii)). The screening charges would continuously modify until reaching the maximum level of strain before achieving a new electrostatic equilibrium (Fig. 9b(iii)). Correspondingly, as polarization was enhanced under stress, the combined charge density would increase with more adsorbed screening charges on the surface. Simultaneously, carriers of opposite polarity would participate in the generation of ROS (Fig. 9b(iv)). Piezoelectric materials utilized piezoelectrically driven potential as the driving force, while oscillating mechanical forces continuously catalyzed the release and adsorption of redox reactions of screening charges [111,112].

The efficiency of piezoelectric catalyzed ROS generation essentially depends on the piezoelectric coefficient, and typically, piezoelectric catalytic activity increases with the increase in piezoelectric coefficient. Classic piezoelectric

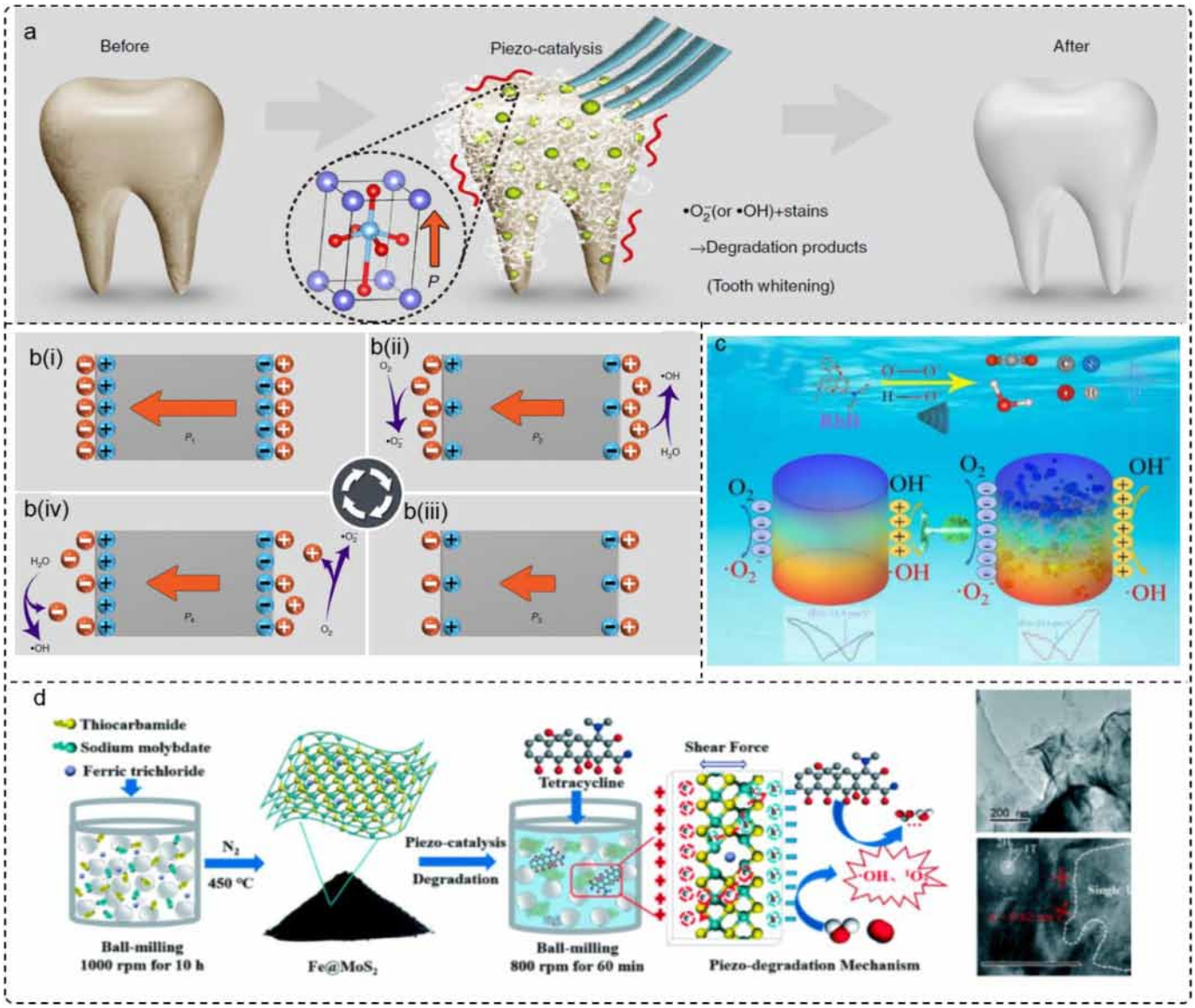

Fig. 9. **Screening charge effect in piezochemistry.** (a) The proposed piezocatalysis effect based tooth whitening method wherein piezoelectric particles replace traditional abrasive in the toothpaste, to generate ROS via piezocatalysis to bleach tooth stains. Reprinted with permission from Ref. [110]. Rightslink® by Creative Commons Attribution 4.0 International. (b) The detailed mechanism of piezocatalysis effect. Reprinted with permission from Ref. [110]. Rightslink® by Creative Commons Attribution 4.0 International. (c) Mechanism diagram of piezoelectric catalysis of ZnO NRs and holey ZnO NRs. Reprinted with permission from Ref. [115]. Rightslink® by Creative Commons Attribution 4.0 International (d) Schematic of the preparation of Fe@MoS_2 and piezo-degradation of tetracycline. Reprinted with permission from Ref. [121]. Rightslink® by Copyright Clearance Center.

materials proven to be used as piezoelectric catalysts include inorganic $BaTiO_3$, ZnO, and $BiFeO_3$, as well as organic polyvinylidene fluoride (PVDF) [113,114]. The advantages of ZnO include good chemical stability, high catalytic activity, high reusability, low cost, non-toxic, environmentally friendly, etc. ZnO rods can generate surface charges under an external mechanical force, triggering electrochemical reactions and realizing energy conversion. Li et al. employed the built-in nanopores in singlecrystal ZnO rods (holey ZnO NRs) to form stress to intensify piezo-catalytic efficiency (Fig. 9c) [115]. The piezoelectric coefficient of holey ZnO NRs increased by 1.92 times than that of the ZnO rods without built-in nanopores (ZnO NRs). The enhanced piezoelectric coeffect of holey ZnO NRs triggered the amplification of piezoelectric catalytic property, which was about 1.7 times that of ZnO NRs. This work demonstrated that the method of induced stress with built-in nanopores was a promising strategy for improving the piezoelectric catalytic efficiency of single-crystal ZnO rods.

5.3. Repeatability of piezomaterial in piezochemistry

In addition to high degradation activity, the repeatability and stability of piezoelectric materials are also crucial for expanding their engineering applications. However, current research findings suggested that mechanical activation could disrupt the microstructure of piezoelectric materials, leading to a decrease in piezoelectric catalytic activity and stability [116]. To overcome this limitation, numerous studies had been conducted. Wu et al. discovered that the introduction of $NaNbO_3$ could significantly enhance the piezoelectric activity, durability, and stability of ZnO catalysts [117]. Wu et al. reported the synthesis of PDMS/WS_2NF using PDMS embedded with richly layered WS_2 nanoflowers, exhibiting stable piezoelectric catalytic performance in degrading RhB dye [118]. After ten cycles of testing, the degradation efficiency of RhB was maintained at approximately 82%. Recently, Kubota et al. demonstrated that piezoelectric materials with temporarily highly polarized particles could be produced through ball milling [119]. Interestingly, Meng et al. found that the piezoelectric catalytic activity and reusability of few-layer WS_2 could be significantly improved by self-renewing [120]. Additionally, Meng et al. synthesized a friction-positive Fe@MoS_2 piezoelectric catalyst with significantly prolonged lifespan through a simple mechanochemical process (Fig. 9d) [121]. The prepared Fe@MoS_2 exhibited excellent piezoelectric catalytic activity activated by ball milling. Wet ball milling was used as the driving force to successfully eliminate the destruction of its piezoelectric catalytic sites. After 50 cycles of testing, Fe@MoS_2 maintained a piezoelectric degradation efficiency of over 99% for tetracycline. Free radical quenching results and electron paramagnetic resonance spectra indicated the generation of $\cdot OH$ and $^1O_2$, which participated in the degradation of tetracycline. Moreover, the toxicity of most intermediates, from the piezoelectric catalysis of Fe@MoS_2, was significantly lower than that of tetracycline, suggesting the potential of Fe@MoS_2 in reducing wastewater toxicity. It provided a deeper understanding of the role of loaded iron in piezoelectric catalysis and offered a new perspective for effectively reducing the quantity and toxicity of antibiotics in water through practical piezoelectric catalytic degradation.

6. Reactions induced by CE effect

Although piezochemistry finds widespread application in numerous significant mechanochemical reactions [119], its limited selection of piezoelectric materials has somewhat constrained further advancements in this field. Additionally, commonly used piezoelectric materials, such as $BaTiO_3$ and lead zirconate titanate (PZT), are brittle [122], environmentally harmful due to their lead content, and challenging to recycle [123]. Moreover, the piezoelectric polar charged state is typically transient, reverting to an uncharged state once the external force is removed and electron–hole pairs recombine [124]. However, it is noteworthy that insulating dielectric solid materials, selected from a broad spectrum, have attracted considerable attention for their ability to facilitate chemical reactions via the ubiquitous Contact Electrification (CE) effect [125]. Once two objects come into contact under mechanical force, a significant charge transfer occurs at the interface, establishing a strong electric field in the separation space upon their separation, thereby enhancing the efficiency of chemical reactions [126]. More recently, most of studies demonstrated the dominance of electron transfer in the CE process [127–129], which strongly supported the feasibility of CE induced reactions [130]. Furthermore, with the advantages of a diverse range of CE materials, cost effectiveness, and stable properties, the research on CE induced chemical reactions has gained increasing attention [131,132]. Chemical reactions induced by the CE effect can be broadly classified into two categories: (1) Reactions driven by surface charges on triboelectrically charged insulating dielectric solids; (2) Reactions initiated by the CE process between insulating dielectric solids and liquids, primarily involving electron transfer and radical generation.

6.1. Reactions induced by electrostatic charge

Liu et al. reported that charged PTFE could engage in reactions with solution species [133]. Specifically, PTFE, negatively charged via CE with PMMA, initiated chemical reactions when immersed in an aqueous solution. These reactions included a pH increase, hydrogen gas formation, metal deposition, reduction of $[Fe(CN)_6]^{3-}$, and chemical luminescence in the $Ru(bpy)_3^{2+}/S_2O_8^{2-}$ system (Fig. 10a and b). Since such phenomena were similar to electron transfer reactions observed in electrochemistry with metal electrodes, charged PTFE could be used for “single-electrode” electrochemical reduction reactions [134]. Furthermore, Liu et al. reported that the $[Fe(CN)_6]^{3-}$ could be reduced to $[Fe(CN)_6]^{4-}$ by the negatively charged polyethylene (PE) that CE with polyamide (PA). (Fig. 10c) Additionally, Liu et al. demonstrated that pristine PMMA could spontaneously transfer electrons to

substances in the aqueous solution, initiating various chemical reactions [135]. The transferred charges were termed cryptoelectrons, somewhat analogous to "excess electrons" on oxide dielectrics. Their surface density was approximately 5×10^{13} cm^{-2}, possessing significantly more negative reduction potentials compared to the bonded electrons in PMMA. Metal ions including Ag^{+}, Cu^{2+} (Fig. 10d), and Pd^{2+} were reduced and plated onto the surface of PMMA, and $[Fe(CN)_6]^{3-}$ was reduced to $[Fe(CN)_6]^{4-}$. Furthermore, when PMMA powder was dropped into a weakly acidic solution, protons were reduced, leading to an increase in pH and the generation of hydrogen gas. Adding PMMA powder to a solution containing $Ru(bpy)_3^{2+}$ and $S_2O_8^{2-}$ also produced chemical luminescence reactions. These results clearly indicated the presence of available electrons in PMMA, capable of participating in redox reactions at substantially negative potentials.

The total net charge of polymer samples can be measured directly and with high precision using Faraday cups. This measurement represents the arithmetic sum of net negative and positive local surface domains. A dielectric solid with a net charge of -1 nC (equivalent to the charge of 6.24×10^9 electrons) may carry significantly larger localized charges. Importantly, the degree to which the sample acts as an electron source far exceeds the net charge measured in Faraday cups/electrostatic meter setups. Zhang et al. demonstrated that CE encompasses an intricate mosaic of positive and negative charges, rather than a homogeneous entity, thereby pioneering the quantitative characterization of these charges within the realm of electrochemistry. They also provided circumstantial evidence for lateral charge migration on dielectric solid surfaces towards metal nanoparticle nucleation sites, as well as inhomogeneous charge densities across the dielectric surface. Additionally, they demonstrated a material-specific slope in the redox work versus electrostatic charge density curves, highlighting the necessity of considering a sensitivity factor when utilizing dielectric solids to deliver a precise amount of coulombs to a reaction mixture. Materials characterized by a substantial negative electron affinity and relatively low ionization energies, which favor stable cations and unstable anions, could effectively facilitate redox processes to a considerable degree. Dielectric solids with stable anions (less negative electron affinity) and large ionization energies will probably be of greater importance when one attempts to deliver small redox changes with high precision. (Fig. 10e) [136]. The maximal magnitude of redox reaction also depends on the material: metal particles undergo greater growth on charged dielectric solids, resulting in the formation of stable cationic fragments with lower ionization energies.

While the phenomenon of inducing chemical reactions through contact with charged dielectric solids has garnered widespread attention among researchers, its origins remain largely obscure. To date, it is commonly believed that this effect arises from an excess of electrons generated on the negatively charged surface, which subsequently transfer to reactants in the solution. The involvement of so-called "cryptoelectrons," as proposed by Liu et al. [135], namely high-energy state electrons existing on or near the surface of the polymer, has been proposed. In these studies, various sources of these electrons had been suggested, including impurities or additives within the dielectric solids, reactive end groups of the dielectric solids, cosmic rays, and surface states induced by the unique status or mechanical fracture of dielectric solids chains. However, works by Lubomirsky et al. cast doubt on the participation of cryptoelectrons in driving solution reactions. Specifically, they replicated several PMMA/PTFE CE experiments and employed X-ray photoelectron spectroscopy (XPS) to demonstrate that negatively charged PTFE did not reduce Pd^{2+} or Cu^{2+} salts but rather facilitated the adsorption of metal cations [137]. While the influence of plasma (utilized for cleaning the polymers) in their study had also sparked some debate over these findings [138]. Baytekin et al.'s research findings on reactions involving free electron transfer suggested that during CE processes, the contacting materials did not uniformly charge but rather form a "mosaic" of positive and negative charges on both contacting surfaces (Fig. 10f). Consequently, both surfaces, not just those with a net negative charge, should be capable of providing electrons. In fact, each charged surface exhibited a "mosaic" of nano-sized (+) and (−) regions, and the total charge of the macroscopic material corresponded to the sum of charges over these domains [139]. Since each nano-domain carried a high charge (approximately μC cm^{-2}) theoretically, each (−) region on a charged dielectric solid contact patch could provide sufficient electrons to drive redox reactions in the surrounding solution. Thus, macroscopic measurements of charged materials (e.g., via Faraday cups) alone cannot conclusively prove or refute whether electrons mediate reactions influenced by contacted charged dielectric solid. It also suggested that reactions induced by dielectric solid surfaces are not attributable to electron (or free electron) reduction but rather to the presence of free radicals [140], which are generated concomitantly with surface charging and material transfer during contact and separation processes.

Prior research has predominantly focused on electrostatic charges on dielectric solids, making direct observation of potential in the aqueous phase as a driving force for redox reactions unattainable. Indirect measurements, relying on concentration changes triggered by dielectric solid redox reactions, have been used as proxies for assessing the extent of these reactions at equilibrium. However, discerning between reactant adsorption and reduction remains unclear, leading to controversial results. Yun et al. investigated the electrostatic and electrochemical behavior of conductive gold, which acquired charge upon contact with the insulating PDMS [141]. This study was motivated by several factors: (1) clarifying electrostatic charges on the conductive phase of gold to elucidate the prevailing mechanism (charge or ion transfer); (2) evaluating the interface potential difference between charged gold and electrolyte using the Nernst equation to gain direct insights into the driving force for electrostatic charge redox reactions; and (3) accurately quantifying charges and adsorbates through stripping voltammetry and surface-sensitive electrochemistry to deepen understanding of redox reactions facilitated by CE. Initially, Au was charged by simple

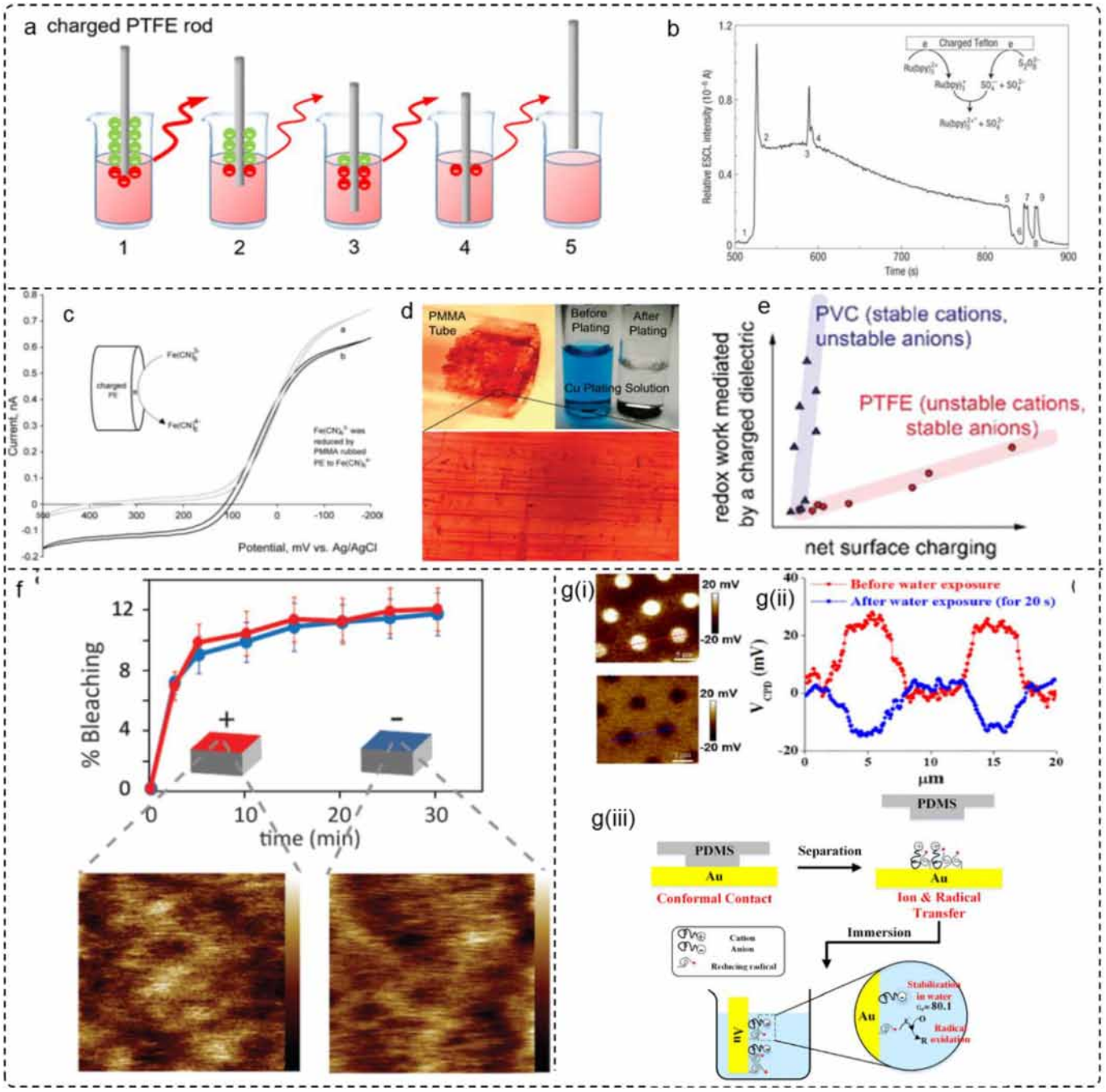

Fig. 10. **Reactions induced by electrostatic charge.** (a) Electrostatic electrochemiluminescence induced by a negatively charged PTFE rod. Reprinted with permission from Ref. [126]. Copyright (2021) by Copyright Clearance Center. (b) The electrochemiluminescence emission phenomenon of electrostatic electrochemiluminescence. Reprinted with permission from Ref. [134]. Copyright (2008) by Copyright Clearance Center. (c) Cyclic voltammograms (10 mV s^{-1}) at a 23 lm glass-encased Pt ultramicroelectrode in water containing 0.2 mmol L^{-1} $[Fe(CN)_6]^{3-}$ and 0.2 mol L^{-1} KCl before (grey) and after (black) contact with PMMA rubbed PE disks. Reprinted with permission from Ref. [133]. Copyright (2010) by Copyright Clearance Center. (d) Copper plated on untreated PMMA surface. Reprinted with permission from Ref. [135]. Copyright (2009) by Copyright Clearance Center. (e) An almost linear relationship between a plastic sample's net negative charge and the amount of solution metal ions discharged to metallic particles with a coefficient of proportionality linked to its electron affinity (stability of anionic fragments). Reprinted with permission from Ref. [136]. Copyright (2019) by Copyright Clearance Center. (f) Kinetics of % bleaching of Neutral Red (NR) aqueous solutions by PDMS charged negatively by rubbing against PC (red line) and charged positively by rubbing against Teflon (blue line). Reprinted with permission from Ref. [139]. Copyright (2012) by Copyright Clearance Center. (g(i)) VCPD images before (top left, 25.9 ± 3.1 mV) and after (bottom left, −13.9 ± 1.3 mV) water exposure. (g(ii)) The corresponding Line profiles of the VCPD. (g(iii)) Illustration of proposed mechanism for electrification and redox reaction in aqueous phase. Reprinted with permission from Ref. [141]. Copyright (2018) by Copyright Clearance Center.

contact and separation with PDMS. Given the extremely low surface energy and inertness to chemicals, PDMS had been widely used as a stamp in soft lithography and microfluidics [142], indicating a low likelihood of chemical interactions between PDMS and Au. Surface potentials measured using Kelvin probe force microscopy (KPFM) in air were utilized to monitor the electrostatic charges on gold. Upon contact with water, the initial positive potential observed on charged Au exhibited a reversal to a negative potential (as shown in Fig. 10g(i)). Subsequently, the study estimated the interface potential difference or Nernst potential based on (1) the open circuit potential (OCP), (2) electrochemical studies of charged Au after redox reactions with electrolyte containing Ag^+ cations using stripping voltammetry, and (3) copper underpotential deposition (UPD) to measure the surface coverage of adsorbates through CE. The focus of this investigation was on the charged Au rather than charged PDMS, to leverage the capability of the conductive phase (equipotential surface) for direct electrical/electrochemical measurements. The OCP result indicated that charged Au has more negative potential than bare Au, and reduction was favorable by the charge transfer between chemicals on Au and $[Fe(CN)_6]^{3-}$. This demonstrated that the charged Au induced reduction from the inverted charges/radicals instead of the oxidation. Apart from charged species, gold may harbor neutral radical species resulting from the homolytic cleavage of the covalent bonds of PDMS [143]. The inverted charge density (1.2 nC cm^{-2}) from −13.9 mV in air in Fig. 10g(ii) was not sufficient to drive chemical reduction. This charge density on gold corresponded to only −0.17 mV in the highly dielectric medium of water, considering the relative permittivity of water (the value of 80.1). Thus, this study speculated that radicals themselves or their anionic derivatives in Fig. 10g(i) may also induce the reduction reaction. As illustrated in Fig. 10g(iii), this study suggested that for the conversion of mechanical energy to chemical reactions, prioritizing radicals generated via mechanochemistry over triboelectricity is advisable.

6.2. Reactions induced by solid–liquid CE

CE at solid–liquid interfaces is also a prevalent phenomenon, alongside solid–solid CE [144]. Some studies had solely attributed the charge transfer process at the solid–liquid interface to ion adsorption or ion transfer stemming from ionization reactions. However, recent research had demonstrated the presence of electron transfer during the CE process at solid–liquid interfaces, indicating that in certain cases, electron transfer was the predominant process [145]. An electron cloud potential-well model had been proposed (Fig. 11a) to elucidate the general scenario of CE between two materials [146]. When two materials interact under external mechanical force, their electron clouds overlap, reducing the energy barrier between them. Sufficient input energy surpasses this barrier, prompting electron transfer from one atom to another. The transferred electrons remain on the receiving atom, suggesting the feasibility of catalyzing chemical reactions via electron transfer in CE.

Moreover, the charge transfer, mainly electron transfer, occurring in solid–liquid CE could be measured by the spatially arranged electrode probes made of self-powered liquid droplet triboelectric nanogenerator (TENG) [147]. Subsequently, Zhang et al. proposed a strategy for electrostatic modulation of chemiluminescence (CL) by CE between reaction solution and dielectric solids (Fig. 11b) [148]. The charged polarity (positive or negative) of luminol droplets, determined by their CE characteristics with various dielectric solids, significantly influenced the reactivity of chemiluminescence. Luminol droplets, positively charged through CE with PTFE, exhibit heightened reaction activity and intensified chemiluminescence. Conversely, luminol droplets negatively charged via CE with nylon tend to suppress chemiluminescence. This phenomenon may arise from electron competition between the negatively charged luminol droplets and Fe^{3+} ions, hindering the chemiluminescent reaction. Fe^{3+} could be reduced by electrons to Fe^{2+} ($Fe^{3+} + e \rightarrow Fe^{2+}$), and Fe^{2+} in alkaline solutions (the pH of the luminol solution in this work is 12) could further be oxidized to form $Fe(OH)_3$ ($4Fe^{2+} + 8OH^- + O_2 + 2H_2O \rightarrow 4Fe(OH)_3$), thereby suppressing CL emission (Fig. 11c). This work provided a strategy to promote/inhibit chemiluminescence by simply statically charging the reaction solution with a dielectric solid, extending our understanding and control of static electricity, with direct implications for triboelectric charge.

In 2022, Wang et al. proposed the contact-electro-catalysis (CEC) strategy for the first time to demonstrate that electrons transferred between original dielectric powders and water during the CE process could be utilized for catalytic reactions without the need for conventional catalysts [149]. Specifically, frequent CE at the interface of fluorinated ethylene propylene (FEP) and water induces electron transfer, triggering the generation of ROS to degrade methyl orange in waste water (Fig. 11d(i)). The cavitation bubbles (CBs) induced by ultrasound was believed to cause frequent contact and separation at the FEP-water interface, facilitating the interfacial electron transfer. As shown in Fig. 11d(ii), CBs initially nucleated during ultrasonic processing. Subsequently, CBs containing dissolved gas grew from the nucleus until reaching a critical size. At this point, the collapse of CBs generated high-pressure microjets, displacing water molecules previously adsorbed on the FEP surface. Electrons transfer from water to FEP upon contact, and the symbol FEP* was introduced to describe the charged state of FEP after separation from water. Simultaneously, upon collision, trapped O_2 was released and captures electrons from the charged surface of FEP*. FEP* returned to its initial uncharged state after exchanging this electron for O_2, and as long as ultrasonication process continues, this electron transfer cycle repeated. Fig. 10d(iii) summarized the potential mechanism of CEC for degrading organic pollutants. On one hand, electron transferred between water and FEP during the CE process led to the formation of water radical cations. The resulting water radical cations underwent rapid proton transfer from water, forming hydrated hydrogen cations and hydroxyl radicals. On the other hand, electrons accumulated on the

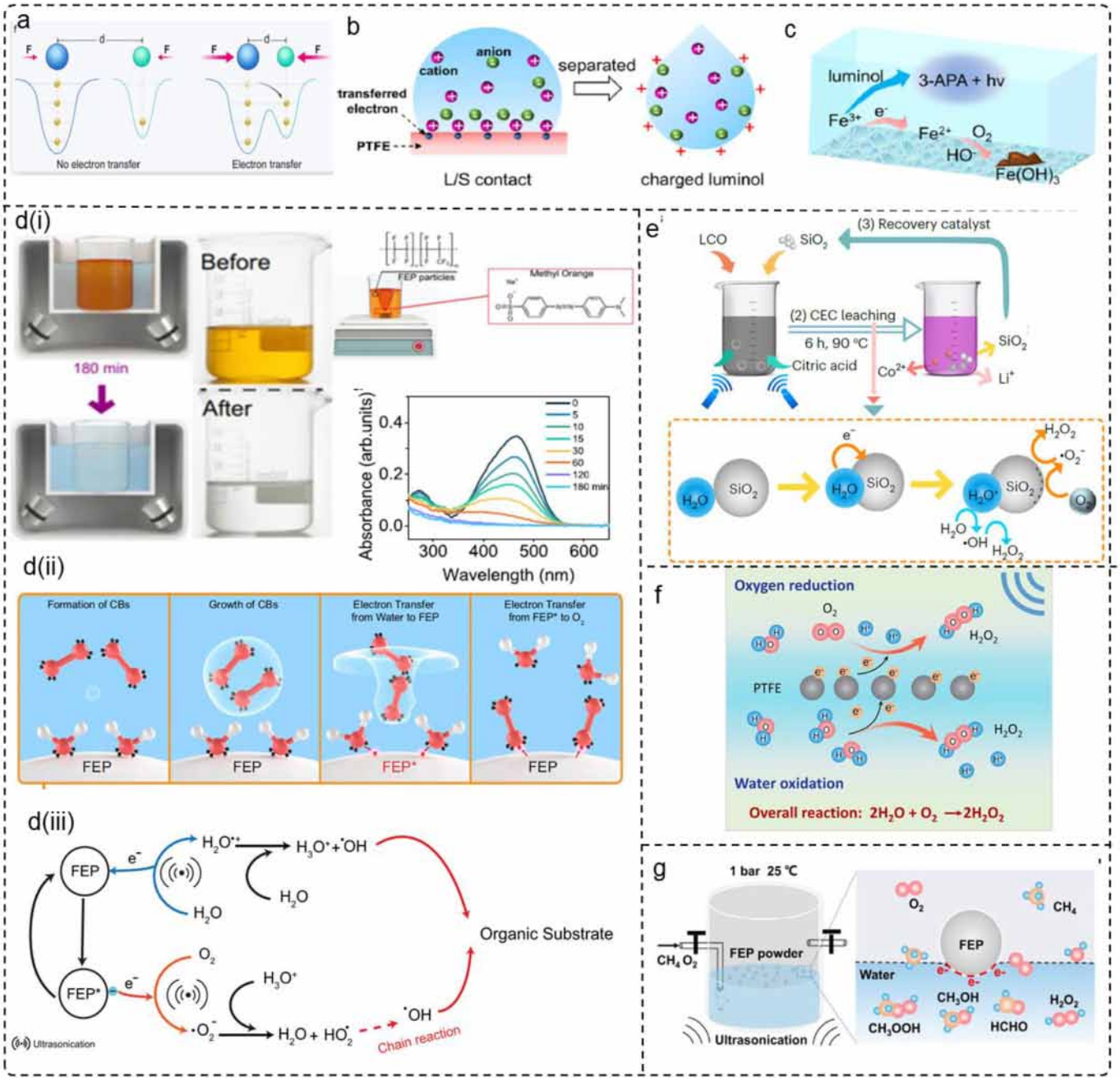

Fig. 11. **Mechanochemical reactions induced by S-L CE.** (a) An electron cloud potential-well model. Reprinted with permission from Ref. [146]. Copyright (2024) by Copyright Clearance Center. (b) Schematic depiction of the electron transfer between a liquid droplet and the PTFE interface and thus the ions adsorbed due to the coulombic attraction. After separation, the positively charged luminol droplet attracts anions at the interface. Reprinted with permission from Ref. [148]. Copyright (2022) by Copyright Clearance Center. (c) Schematic depiction of the electrons from the negatively charged luminol droplet competing with luminol for Fe^{3+}. Reprinted with permission from Ref. [148]. Copyright (2022) by Copyright Clearance Center. (d(i)) Schematic of the experimental setup and protocol of CEC. c UV-Vis spectra of a 50 mL aqueous methyl orange solution during ultrasonication in presence of FEP powder (20 mg) for 3 h (d(ii)) Schematic of the CEC phenomenon during ultrasonication. (d(iii)) Proposed mechanism for the degradation of methyl orange by CEC generated radicals. Reprinted with permission from Ref. [149]. Copyright (2022) by Creative Commons Attribution 4.0 International. (e) The powder and SiO_2 catalyst were put into citric acid solution under ultrasonic conditions. Reprinted with permission from Ref. [151]. Copyright (2023) by Copyright Clearance Center. (f) Mechanism of CEC to generate H_2O_2. Reprinted with permission from Ref. [152]. Copyright (2023) by Copyright Clearance Center. (g) Schematic diagram and reaction pathway of the oxidation of CH_4 to HCHO and CH_3OH via CEC. Reprinted with permission from Ref. [153]. Copyright (2024) by Copyright Clearance Center.

FEP* surface were captured by O_2, forming $\cdot O_2^-$ radicals. Subsequently, $\cdot O_2^-$ was protonated to form hydroperoxyl radicals ($HO_2\cdot$), which, generate $\cdot$OH radicals through chain reactions [150]. $\cdot$OH radicals produced at the end of these two steps then reacted with organic pollutants in the aqueous solution. CEC had been demonstrated to be effective with various dielectric materials such as Teflon, Nylon-6,6, and rubber. This original catalytic principle not only broadened the

scope of catalytic materials but also allowed us to envision catalytic processes facilitated by mechanically induced CE.

CEC, utilizing electron transfer and free radical generation during contact electrification between diverse materials, efficiently degrades organic pollutants and retrieves electrode materials from lithium-ion batteries. Li et al. harnessed the generation of radicals from CEC approach to facilitate metal leaching under ultrasonication [151]. SiO_2 was employed as a recyclable catalyst in CEC. For lithium cobalt oxide (III) batteries, lithium leaching efficiency reached 100% within 6 h at 90 °C, while cobalt leaching efficiency reached 92.19%. In the case of ternary lithium batteries, within 6 h at 70 °C, the leaching rates for lithium, nickel, manganese, and cobalt reached 94.56%, 96.62%, 96.54%, and 98.39%, respectively. This method offered a green, efficient, and cost-effective approach for lithium-ion battery recycling, meeting the exponential growth in demand for lithium-ion batteries. The entire recycling process was illustrated in Fig. 11e, lithium cobalt oxide (LCO) was first separated from lithium-ion batteries (LIBs), followed by metal extraction through CEC leaching. After a 6-h reaction, the solution turned pink, indicating successful metal leaching from the cathode material. Then the metals were separated through continuous precipitation, and the catalyst (SiO_2) was recovered. Ultrasonication induced the growth and collapse of cavitation bubbles, leading to frequent CE between SiO_2 and the water interface. Consequently, electrons transfer from DI water to the SiO_2 surface. This process generated hydroxyl radicals cations, which reacted with water molecules to form ·OH and hydrated hydrogen ions. During the collapse of cavitation bubbles, oxygen present in the bubbles reacted with electrons on the SiO_2 surface, forming $\cdot O_2^-$. Electrons, superoxide species, and hydroxyl radicals all potentially participated in the leaching process. Finally, a precipitation method was employed to separate the mixture of lithium and cobalt ions from the solution.

Zhao et al. had proposed a straightforward method for the direct production of hydrogen peroxide (H_2O_2), based on CE between PTFE particles and deionized (DI) water, without the need for any other traditional catalysts such as noble metals, intermetallic alloys, and transition metal oxides [152]. Under ultrasonication treatment, electron transfer occurred between PTFE particles and water, with repeated contact and separation cycles at the interface. Electrons could flow from water to the surface of PTFE, forming a charged interface, effectively catalyzing chemical reactions that typically did not occur under ambient conditions. Electron paramagnetic resonance (EPR) was employed to capture intermediate radical species (·OH and $\cdot O_2^-$). As shown in Fig. 11f, the contact between PTFE and water and the PTFE-O_2 interface triggered electron transfer and also might generate radicals, so that the recombination of radicals produces H_2O_2, with a yield of up to 313 μmol L^{-1} h^{-1}. Furthermore, the influence of locally elevated pressure environments induced by ultrasonication on the reaction was investigated through theoretical simulation methods. Through Raman spectroscopy, scanning electron microscopy (SEM), and X-ray photoelectron spectroscopy (XPS) that the surface structure and chemical composition of PTFE particles remained unchanged during the ultrasonic treatment. This physical and chemical stability might favor the large-scale production of H_2O_2. Therefore, we proposed a simple and cost-effective production system based on the principles of CEC, which achieved long-term stable performance and held promise for application in various systems, pioneering new frontiers in catalysis.

Recently, Li et al. demonstrated that CEC could effectively catalyze the direct synthesis of H_2O_2 under ambient conditions, concurrently generating abundant reactive oxygen intermediates [153]. H_2O_2, as an oxidant, had been shown to effectively oxidize methane (CH_4) under mild conditions. Ultrasonication was utilized to facilitate CE between FEP particles and water to catalyze the oxidation of CH_4 to formaldehyde (HCHO) and methanol (CH_3OH) under ambient conditions, with yields of 467.5 and 151.2 μmol $gcat^{-1}$, respectively. The reaction was conducted at 25 °C and 1 bar pressure under ultrasonic treatment (Fig. 11g). In the presence of ultrasound, water contacted and separated from the FEP surface. Due to the strong electron-absorbing capability of FEP, H_2O lost electrons to form ·OH, while electrons were adsorbed onto the FEP surface to form static charges. In the presence of cavitation bubbles, oxygen gained electrons and was activated into ·OOH. These oxygen radicals further activated CH_4. The FEP surface, upon receiving electrons, activated O_2 in a negatively charged chemical environment and combined with hydrated hydrogen ions to form ·OOH. Additionally, the catalyst used in CEC was readily available, exhibiting good universality, durability, recyclability, and scalability for CH_4 conversion. The significance of this method and its potential applicability to a wider range of gas-phase catalytic reactions underscored significant advancements in the catalysis field.

CEC has facilitated the development of non-metallic catalytic methods for efficiently degrading persistent organic compounds, producing hydrogen peroxide, and recovering metals from spent lithium-ion batteries. Su et al. demonstrated the application of CEC principles in devising a non-metallic catalytic route for the reduction of precious metals in aqueous solutions [154]. FEP particles, owing to their high CEC activity, could drive CEC-mediated reduction of gold (Au), mercury (Hg), palladium (Pd), platinum (Pt), iridium (Ir), rhodium (Rh), and silver (Ag) ions in aqueous solutions under both aerobic and anaerobic conditions (Fig. 12a). More significantly, this water-solid CE-based method enabled the extraction of gold from synthetic solutions with concentrations ranging from as low as 0.196 ppm to as high as 196 ppm, with extraction capacities ranging from 0.756 to 722.5 mg g^{-1} in 3 h. Fig. 12b depicted a schematic diagram of the mechanism of metal ion reduction via CEC. Following ultrasound-assisted water-solid CE, the charged FEP (denoted as FEP*) emitted electrons into the solution under the excitation provided by ultrasonic vibration. These electrons could reduce the metal ions present in the solution. After the electrons departed from FEP*, the latter returns to its ground state (FEP), and if the ultrasound conditions were maintained, the catalytic cycle as a method for extracting metals from aqueous solutions, CEC

offered several advantages. The widespread availability of high-performance dielectric insulating fluoropolymer and ceramic particles resolves common challenges related to contamination experienced by novel catalysts. Due to the chemical inertness of fluoropolymer, the extracted metals precipitated at the bottom of the reactor rather than being fixed on the catalyst, floating on the surface. This facilitated the recovery of the desired compounds compared to adsorbent processes requiring further post-treatment (i.e., selective dissolution and reprecipitation). Moreover, CEC metal reduction allowed for metal recovery from solutions with low pH values, such as industrial filtrates obtained from electroplating waste. Due to significant differences in the reduction kinetics of gold and other metals, CEC enabled the selective recovery of gold from filtrates of the same waste solution. Lastly, the physicochemical properties of FEP conferred excellent recyclability to this material. Future research endeavors should prioritize optimizing CEC efficiency, identifying low-contamination materials, and exploring the broader spectrum of reactions achievable through this method. Furthermore, investigating CEC's potential across diverse catalytic and mechanochemical processes remains paramount.

The essence of initiating CEC relies on introducing effective contact-separation cycles at the target interface. During these cycles, electron transfer is expected to facilitate the rate of chemical reactions. Ultrasound is commonly used to induce CEC, exploiting the variation in cavitation bubbles during the propagation of ultrasound waves to generate high-pressure microjets, thereby causing contact-separation cycles between solids and liquids and the corresponding electron transfer. Additionally, ultrasound treatment can not only induce high-frequency CEC but also provide a high-pressure environment, thereby promoting the generation of reactive ROS by reducing the energy barrier for electron transfer. These ROS can effectively degrade organic pollutants or directly synthesize H_2O_2. In addition, ball milling is another representative strategy applied in CEC. Wang et al. explored its feasibility through a LAG device made from triboelectric materials (Fig. 12c) [155]. They proposed the existence of a velocity threshold to initiate CEC. Specifically, when the rotation speed was low, the energy for electron transfer during the CE process was insufficient. Further increasing the rotation speed would lead to an increased rate of ROS generation. This could be explained by the increase in impact frequency at higher speeds and the reduction in the energy barrier for interface electron transfer.

Additionally, Zhao et al. proposed a highly sensitive strategy to investigate electron transfer and free radical generation during solid–liquid contact processes [156]. In this approach, small droplets were propelled by a nitrogen flow through a long capillary to provide continuous solid–liquid contact, which could generate a sufficiently high concentration of free radicals within the droplets without the need for ultrasound assistance (Fig. 12d). The results indicated that the free radicals produced without ultrasound are ·OH, formed by the loss of an electron from hydroxide ions (OH^-) during the solid–liquid interface CE process. It was worth noting that no $\cdot O_2^-$ was detected during the solid–liquid contact process. However, after the introduction of ultrasound, $\cdot O_2^-$ was noticeably detected, confirmed that the use of ultrasound did indeed interfere with the electron transfer process and interface reactions. Furthermore, with the assistance of ultrasound, the concentration of ·OH also significantly increased. Additionally, ultrasound-assisted free radical generation could be used to degrade tetracycline contamination. Besides, Zhang et al. proposed a wind-driven, Al@Al_2O_3 and PTFE combined rotational mode liquid–solid TENG CEC and adsorbable device (Fig. 12e) [157]. The CE of the liquid–solid interface during mechanical rotation made the treatment efficiency of organic pollutants much higher than other advanced oxidation processes. Taking crystal violet (CV) as the target pollutant, when the linear speed of the rotator is 1.41 m s^{-1}, the k values for low-concentration and high-concentration crystal violet are 2.24 min^{-1} and 0.26 min^{-1}, respectively. This was a huge advance in the field of catalysis.

Due to the manipulable nature of the CE process and its correlation with the electronegativity of solid dielectrics, it provides a mechanism for controlling chemical reactions and a reliable platform for studying solid dielectric-liquid interactions. Generally, the electron acceptance/donation ability of solid dielectrics in the CE process is closely related to their electronegativity, which depends on the electron affinity of atoms in their chemical structure, similar to the electron theory in the Lewis acid-base law. Combining the work function of charge collectors and the standard electrode potential of electroactive substances in the liquid, the electronegativity of solid dielectrics in the triboelectric series could serve as a benchmark for predicting the thermodynamics of CE-Chemical reactions. Therefore, we proposed a guideline for the unified concept of work function, electronegativity in the triboelectric series, and standard electrode potential to guide chemical reactions and assess their extent. Defining order parameters by electron transfer capability could not only provide a new way to steer chemical reactions via triboelectric charges, but also offer a new perspective to develop a green and sustainable chemistry with interdisciplinary subjects of physics and material science. Furthermore, we introduced the comprehensive paradigm of contact-electro-chemistry (CE-Chemistry), demonstrating that chemical reactions can be driven by free radicals that initiated during the CE process of solid dielectric-liquid (Fig. 12f) [158]. CE-Chemistry covered a wide range of chemical disciplines, including contact-electro-redox (CE-Redox) reactions of $[Fe(CN)_6^{3-}/[Fe(CN)_6]^{4-}$, contact-electro-polymerization (CE-Polymerization) of aniline, contact-electro-catalysis (CE-Catalysis) of phenol, and contact-electro-fluorescent (CE-Fluorescent) of terephthalic acid (THA), and so on. Exploring the formation of the electrical double layer (EDL) elucidates the electron-ion transfer relationship and optimizes CE-Chemistry reactions in aqueous systems. Moreover, CE-Chemistry has been conducted for the first time in non-aqueous environments, underscoring the universality of CE-Chemical mechanisms beyond aqueous systems. Unlike chemical reactions initiated by light, heat, electricity, or chemicals, CE-Chemistry based on mechanical contact-separation methods opens new avenues for

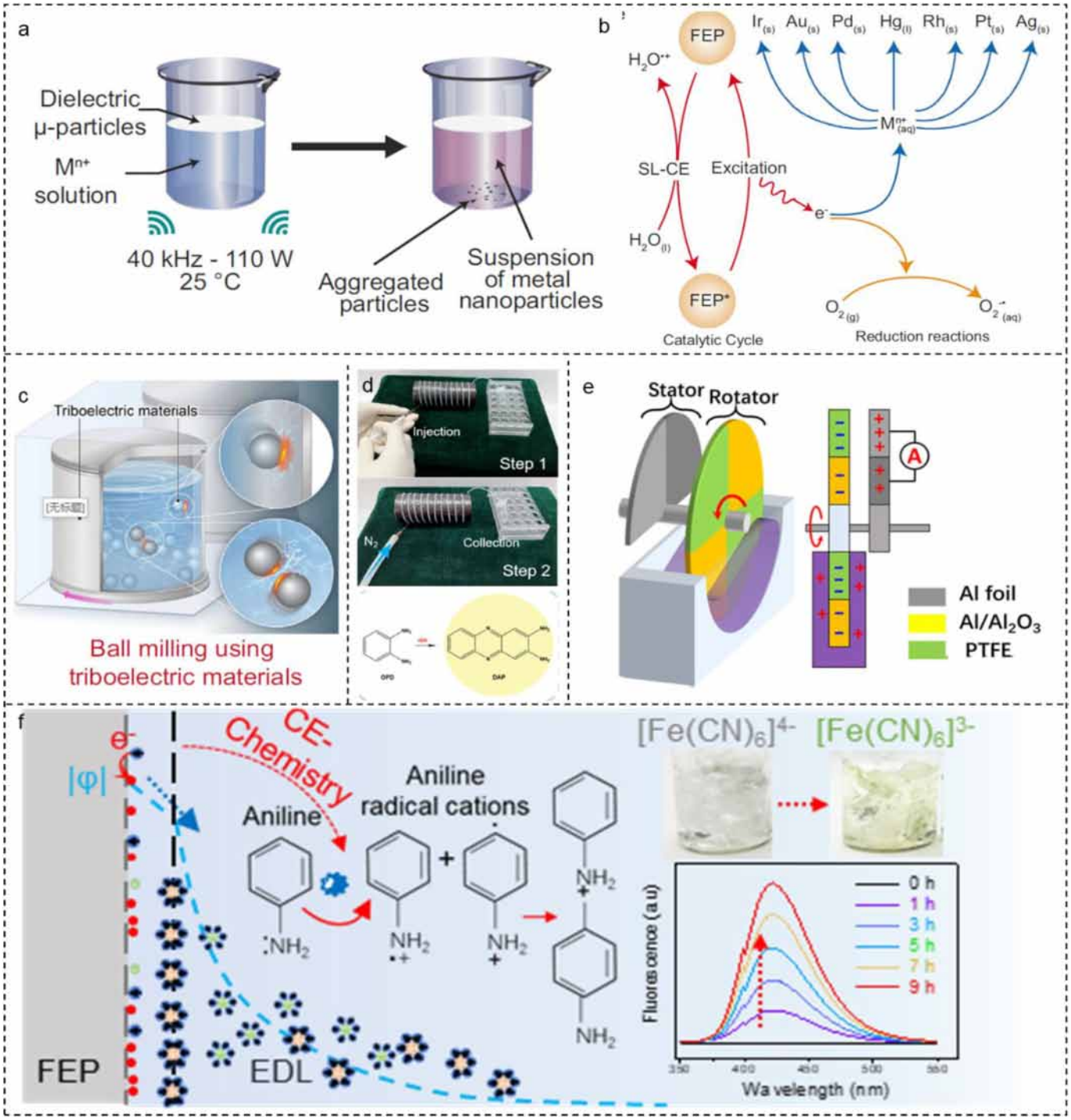

Fig. 12. **Mechanochemical reactions induced by S-L CE.** (a) Reduction of metal ions in solution by ultrasonication in presence of FEP microparticles. Reprinted with permission from Ref. [154]. Copyright (2024) by Copyright Clearance Center. (b) Schematic description of the reduction of various metal ions (M^{n+}) in aqueous solution by ultrasonically driven CEC in presence of FEP. Reprinted with permission from Ref. [154]. Copyright (2024) by Copyright Clearance Center. (c) Production of ROS via contact-electrocatalysis (CEC) in ball milling. Reprinted with permission from Ref. [155]. Copyright (2024) by Copyright Clearance Center. (d) Generation of ·OH induced by CE at solid–liquid interface. Reprinted with permission from Ref. [156]. Copyright (2023) by Copyright Clearance Center. (e) Rotation-mode liquid–solid triboelectric nanogenerator for efficient CEC and adsorption. Reprinted with permission from Ref. [157]. Copyright (2023) by Copyright Clearance Center. (f) A green approach to induce and steer chemical reactions using inert solid dielectrics. Reprinted with permission from Ref. [158]. Copyright (2024) by Copyright Clearance Center.

interdisciplinary research on interface interactions across physical, materials science, and chemistry domains.

Furthermore, the CE-Chemistry and CEC could couple other effects for enhanced chemical reactions. It significantly broadens the range of catalyst selection, enabling the possibility of designing more diverse catalytic systems. Jiang et al. prepared a novel contact piezoelectric dual-catalytic ZnO@PVDF composite membrane using electrospinning technology (Fig. 13a) [159]. The resulting ZnO@PVDF composite membrane outperformed pure PVDF membrane in the ultrasound decomposition of methyl orange (MO) at room temperature, primarily due to the synergistic effect of the contact-electrocatalysis of dielectric PVDF and the piezoelectric catalysis of tetrapod ZnO and α-phase PVDF (Fig. 13b). The heterostructure of piezoelectric-ZnO@dielectric-PVDF composite material was advantageous in reducing electron/hole recombination. The catalytic degradation efficiency of the ZnO@PVDF composite membrane under ultrasound treatment increased by 444.23% compared to pure PVDF membrane. Additionally, the reusability and stability of the composite membrane were comparable to traditional powder catalysts. This study was based on exploring the high degradation efficiency of MO solution under ultrasound treatment using electrospun ZnO@PVDF composite membrane. Under the dual catalytic action of contact piezoelectricity, the prepared ZnO@PVDF composite membrane generated a large number of electrons at the interfaces of PVDF-water and ZnO-water. PVDF, as a dielectric material, can timely store the electrons generated by the contact-electric and piezoelectric effects, prolonging the presence of electrons and holes at these interfaces, thereby ensuring the long-term existence of free radicals. As shown in Fig. 13c, when the cavitation bubbles generated by ultrasound burst, they produced high-pressure and high-temperature microjets, impacting the water molecules previously adsorbed on the ZnO@PVDF composite membrane. Water loses electrons to form H_2O^+, which reacted with H_2O to form ·OH and H_3O^+. Upon contact, an electron transferred from water to PVDF, and the symbol PVDF* was proposed to describe the charged state of PVDF after separation from water. Simultaneously, O_2 captured electrons from the charged PVDF* surface. PVDF* transferred this electron to O_2, forming $\cdot O_2^-$. Afterward, PVDF* transferred the electron to oxygen, and PVDF returned to its original uncharged state, catalyzing the reaction. H_3O^+ reacted with O_2 to generate pure water and ·OH. Dissolved O_2 in water exhibited intense vibration under ultrasound, impacting the PVDF surface. Oxygen had the ability to attract electrons from the negatively charged PVDF, leading to the continuous cycling of PVDF between charged and uncharged states. The system continuously generated ·OH, which were the primary reactive species for MO degradation. This work provided a promising strategy for improving pollutant degradation by combining contact-electric catalysis with piezoelectric catalysis.

Additionally, traditional mechanochemical controlled reversible deactivation radical polymerization (RDRP) utilized ultrasound or ball milling to regenerate catalysts, which could lead to side reactions due to high-energy and high-frequency stimulation. Wang et al. proposed a simple friction-induced chemical control ATRP (tribo-ATRP) method (Fig. 13d),

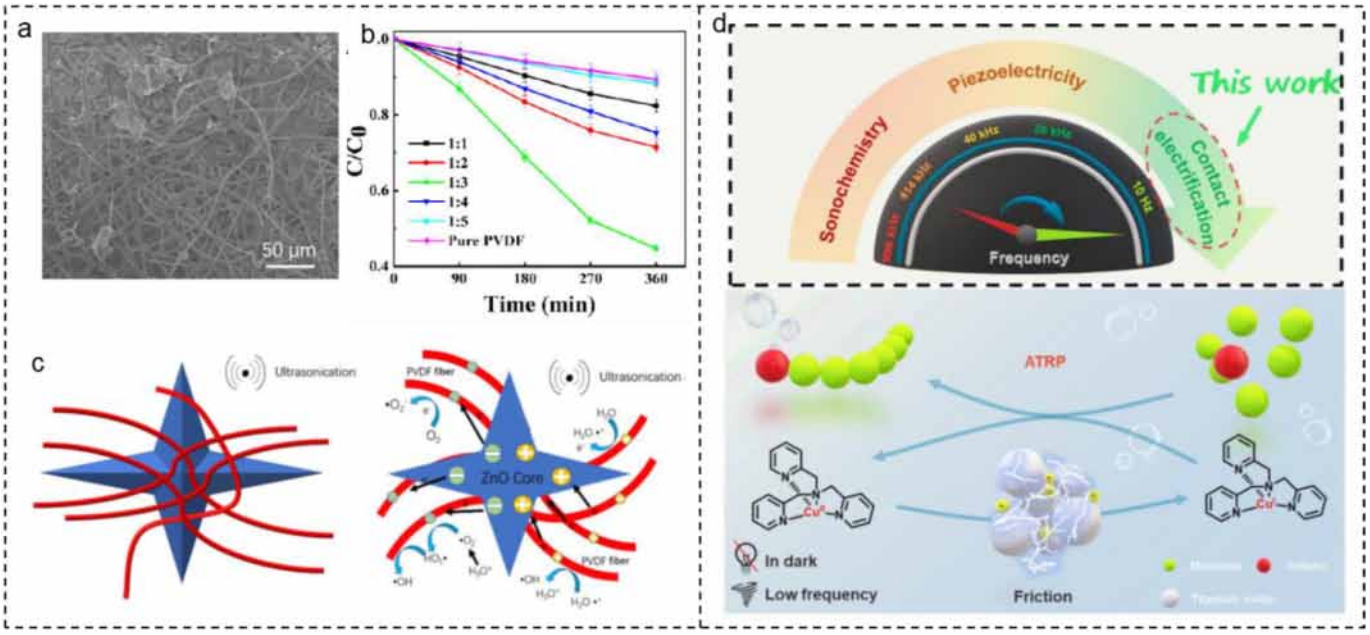

Fig. 13. **Mechanochemical reactions induced by S-L CE and other effects.** (a) The SEM image of ZnO@PVDF composite membrane (ZnO/PVDF = 1:3, w/w). Reprinted with permission from Ref. [159]. Copyright (2022) by Copyright Clearance Center. (b) Decomposition of MO solution at different treatment times using different ZnO@PVDF composite membrane; C_0 and C is the initial and instant concentration, respectively. Reprinted with permission from Ref. [159]. Copyright (2022) by Copyright Clearance Center. (c) Mechanism of the contact-piezoelectric bi-catalysis of MO degradation under ultrasonication. Reprinted with permission from Ref. [159]. Copyright (2022) by Copyright Clearance Center. (d) Proposed mechanism of tribo-ATRP under ultralow frequency stimulation. Reprinted with permission from Ref. [160]. Copyright (2022) by Copyright Clearance Center.

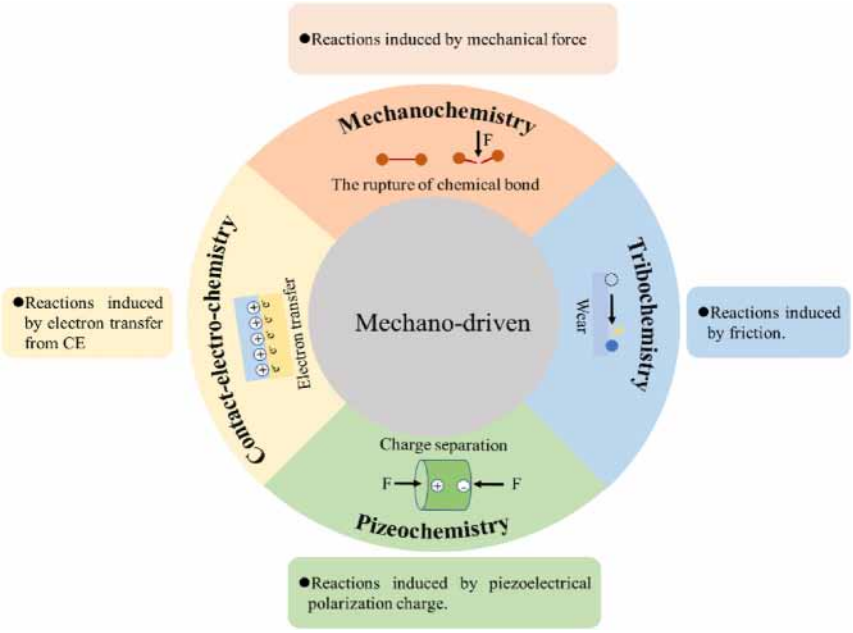

Fig. 14. Mechano-driven reactions with different mechanisms.

which relied on contact-electric catalysis between titanium oxide (TiO_2) particles and $CuBr_2$/tris(2-pyridylmethyl) amine (TPMA), without the need for any high-energy mechanical force [160]. Under stirring-induced friction, TiO_2 particles became charged and continuously reduced $CuBr_2$/TPMA to CuBr/TPMA, converting dormant alkyl halides into active growing radicals, thus initiating ATRP. Additionally, the impact of stirring-induced friction on the reaction was explored through theoretical simulations, indicating that increasing the frequency could lower the energy barrier for electrons to transfer from TiO_2 particles to $CuBr_2$/TPMA. Successful implementation of tribo-ATRP had allowed CEC (~10 Hz) to achieve various polymers with predetermined molecular weights, low disparities, and high chain-end fidelity.

7. Conclusions and perspectives

This article reviews several typical types of mechanically induced chemical reactions, as depicted in Fig. 14, namely mechanochemistry, tribochemistry, piezochemistry, and contact-electric chemistry. Mechanochemistry focuses on the interactions between mechanical energy and chemical reactions. Under the action of mechanical stress, changes in molecular structure, charge distribution, or chemical bonds of substances may occur, leading to the initiation of new chemical reactions or the enhancement of existing ones. These interactions can result in the synthesis of new materials, activation of catalysts, and modulation of biological and chemical processes. However, mechanochemistry remains qualitative and intuitive rather than quantitative and precise. For instance, the mechanics vary by the type of stress involved. Namely, the reaction results under head-on pressure may differ from those under shear stress. Moreover, kinetic effects and thermodynamic effects during mechanochemistry should be separated. The prevalence and importance of localized heating at ball impact locations are also unclear. Therefore, real-time measurements of reactants and products in mechanochemistry are required. Measuring the fractions of different molecules present throughout the mechanical process is crucial for quantifying the reaction dynamics and providing data for modeling. Models that consider the particles as a pseudo-fluid may be help to understand and predict reactions. New techniques and a better theoretical understanding could encourage the commercialization of mechanochemistry.

Tribochemical reactions are profoundly influenced by the concurrent occurrence of friction and mechanical impact, typically accelerating reaction rates and sometimes altering reaction pathways. The technological relevance of tribochemistry spans various applications, including lubricant additive formulation, micro-abrasion in bolt connections, mild wear of metals, mechanically activated reactions in processing industries, seal operation in rotating machinery, and the potential development of novel friction materials. Tribochemistry primarily investigates the chemical reactions induced during friction processes, where surface interactions can lead to the formation, breaking, or transformation of chemical bonds, thereby affecting frictional force and wear behavior. Research in this field advances our understanding of friction phenomena, aids in the development of new lubricants and materials, and enhances the performance of friction interfaces. Despite its potential, the complexity of reaction processes and the demand for higher fidelity and in-situ characterization to better understand and optimize tribochemical processes. Advanced techniques like AFM, transmission electron microscopy (TEM), and the emerging Atomic Probe Tomography (APT) are increasingly utilized to investigate mechanical properties, such as hardness and strength of tribofilm. However, the costs of these advanced techniques outweigh their

benefits, and thus the issue of cost-effective is crucial considering for achieving tribochemistry in efficiency, safety, and sustainability.

Piezochemistry explores the chemical phenomena associated with charge separation or electric field generation under strain or pressure in piezoelectric materials. Research has elucidated two primary mechanisms underpinning piezochemistry: the band theory and the screening charge effect. Both frameworks offer plausible explanations for piezoelectric catalysis, supported by their core principles and empirical evidence. Notably, while both mechanisms highlight the strong correlation between piezoelectric potential and catalytic activity, they differ in the sources of active charge carriers. Proponents of the band theory argue that internally generated charges, resulting from mechanical excitation or material defects, are the primary drivers of reactions. In contrast, the screening charge effect posits that externally released screening charges, stemming from surface shielding phenomena, initiate redox reactions. However, the correlation between piezochemical reaction kinetics and physical mechanisms remains largely unexplored across various aspects. For example, piezoelectric properties are intricately linked to ambient temperatures that will change due to the thermal effects ultrasonication time. Therefore, quantitative analysis is needed to understand the relationship between temperature variations, ultrasonication power density, and duration to effectively manage these thermal effects. Moreover, suppressing the recombination of electron–hole pairs and prolonging the charge carrier lifetime are considered to be the major contributions of piezopotential to photocatalysis.

Unlike the aforementioned types, the CE effect, occurring at interfaces such as solid–solid, solid–liquid, and liquid–liquid, has attracted significant research interest due to its ability to modify surface charge distribution and chemical environment, thereby influencing catalytic activity. By adjusting charge distribution and electric field intensity at contact interfaces, the adsorption capacity and activation energy for reactants on surface catalysts can be controlled, altering reaction rates and selectivity. Furthermore, the electrostatic field generated by CE can drive specific electrochemical reactions by affecting reactant migration rates, electron transfer processes, or activation energies. CEC relies on electron transfer at the solid–liquid interface, generating active radicals that initiate chemical reactions. CE can occur without intense friction and across diverse materials, offering milder conditions and more selective strategies for enhancing reaction rates. However, under mild mechanical conditions, such as stirring or continuous flow at the solid–liquid interface, CE-Chemistry places higher demands on the CE performance of friction materials. Enhancing CE performance can be achieved through physical etching to increase surface area or surface chemical modifications to boost surface charge density. Moreover, designing new CE materials by optimizing their composition, structure, and morphology also holds promise for improving reaction efficiency. Additionally, composite solid dielectrics with varied electron gain and loss capabilities, or metal coatings with diverse electron escape functionalities, can create a built-in electric field, enhancing CE performance. Ongoing research aims to improve reaction efficiency and expand the scope of liquid reaction systems through CEC. Overall, continuous efforts in advancing CE-Chemistry technology are crucial for achieving a more sustainable and greener future.

CRediT authorship contribution statement

Shaoxin Li: Writing − review & editing, Writing − original draft, Visualization, Investigation, Conceptualization. **Jiajin Liu:** Writing − review & editing, Writing − original draft. **Zhong Lin Wang:** Writing − review & editing, Writing − original draft, Supervision, Funding acquisition. **Di Wei:** Writing − review & editing, Writing − original draft, Supervision, Funding acquisition, Conceptualization.

Declaration of competing interest

The authors declare no competing interests.

Acknowledgements

This work was supported by the National Natural Science Foundation (Grant No. 22479016).

References

[1] I. Kita, S. Matsuo, H. Wakita, J. Geophys. Res. 87 (1982) 10789–10795.
[2] J. Telling, E.S. Boyd, N. Bone, E.L. Jones, M. Tranter, J.W. Macfarlane, P.G. Martin, J.L. Wadham, G. Lamarche-Gagnon, M.L. Skidmore, T.L. Hamilton, E. Hill, M. Jackson, D.A. Hodgson, Nat. Geosci. 8 (2015) 851–855.
[3] J. Stone, J.O. Edgar, J.A. Gould, J. Telling, Nat. Commun. 13 (2022) 4529.
[4] L. Takacs, J. Occup. Med. 52 (2000) 12–13.
[5] M. Faraday, Quart. J. Liter, Sci. Arts 8 (1820) 374–376.
[6] L. Takacs, J. Therm. Anal. Calorim. 90 (2007) 81–84.
[7] M.C. Lea, Br. J. Photogr. 13 (1866) 84.
[8] M.C. Lea, Am. J. Sci. 3 (1892) 527–531.
[9] W. Spring, Bull. Soc. Chim. Fr. 40 (1883) 641–647.
[10] A.R. Ling, J.L. Baker, J. Chem. Soc. Trans. 63 (1893) 1314–1327.
[11] W. Ostwald, Nature 107 (1921) 613–615.
[12] L. Takacs, Chem. Soc. Rev. 42 (2013) 7649–7659.
[13] G. Heinicke, H.P. Hennig, E. Linke, U. Steinike, K.P. Thiessen, K. Meyer, M. Cryst. Res. Technol. 19 (1984) 1424.
[14] S.L. James, C.J. Adams, C. Bolm, D. Braga, P. Collier, T. Friščić, F. Grepioni, K.D. Harris, G. Hyett, W. Jones, Chem. Soc. Rev. 41 (2012) 413–447.
[15] X. Hao, D. Feng, P. Huang, F. Guo, Org. Chem. Front. 11 (2024) 2081–2087.
[16] X. Liu, Y. Li, L. Zeng, X. Li, N. Chen, S. Bai, H. He, Q. Wang, C. Zhang, Adv. Mater. 34 (2022) 2108327.
[17] F. Cuccu, L. de Luca, F. Delogu, E. Colacino, N. Solin, R. Mocci, A. Porcheddu, ChemSusChem 15 (2022) e202200362.
[18] R.T. O'neill, R. Boulatov, Nat. Rev. Chem 5 (2021) 148–167.
[19] N. Fantozzi, J.-N. Volle, A. Porcheddu, D. Virieux, F. García, E. Colacino, Chem. Soc. Rev. 52 (2023) 6680–6714.
[20] H. Traeger, D.J. Kiebala, C. Weder, S. Schrettl, Macromol. Rapid Commun. 42 (2021) 2000573.
[21] N. Bruns, K. Pustelny, L.M. Bergeron, T.A. Whitehead, D.S. Clark, Angew. Chem. 121 (2009) 5776–5779.

[22] R. Merindol, G. Delechiave, L. Heinen, L.H. Catalani, A. Walther, Nat. Commun. 10 (2019) 528.
[23] R. Glazier, J.M. Brockman, E. Bartle, A.L. Mattheyses, O. Destaing, K. Salaita, Nat. Commun. 10 (2019) 4507.
[24] S. Ogi, K. Sugiyasu, M. Takeuchi, Bull. Chem. Soc. Jpn. 84 (2011) 40–48.
[25] H. Hu, X. Cheng, Z. Ma, R.P. Sijbesma, Z. Ma, J. Am. Chem. Soc. 144 (2022) 9971–9979.
[26] G. De Bo, Macromolecules 53 (2020) 7615–7617.
[27] M.K. Beyer, H. Clausen-Schaumann, Chem. Rev. 105 (2005) 2921–2948.
[28] J. Li, C. Nagamani, J.S. Moore, Acc. Chem. Res. 48 (2015) 2181–2190.
[29] W.H. Binder, Polymer 202 (2020) 122639.
[30] J.N. Brantley, K.M. Wiggins, C.W. Bielawski, Polym. Int. 62 (2013) 2–12.
[31] M. Stratigaki, R. Göstl, ChemPlusChem 85 (2020) 1095–1103.
[32] D.A. Davis, A. Hamilton, J. Yang, L.D. Cremar, D. van Gough, S.L. Potisek, M.T. Ong, P.V. Braun, T.J. Martínez, S.R. White, Nature 459 (2009) 68–72.
[33] C. Calvino, L. Neumann, C. Weder, S. Schrettl, J. Polym. Sci., Part A: Polym. Chem. 55 (2017) 640–652.
[34] Y. Sagara, H. Traeger, J. Li, Y. Okado, S. Schrettl, N. Tamaoki, C. Weder, J. Am. Chem. Soc. 143 (2021) 5519–5525.
[35] S. Thazhathethil, T. Muramatsu, N. Tamaoki, C. Weder, Y. Sagara, Angew. Chem. 134 (2022) e202209225.
[36] V. Boldyrev, K. Tkáčová, J. Mater. Synth. Process. 8 (2000) 121–132.
[37] P.Y. Butyagin, Russ. Chem. Rev. 53 (1984) 1025.
[38] M.M. Caruso, D.A. Davis, Q. Shen, S.A. Odom, N.R. Sottos, S.R. White, J.S. Moore, Chem. Rev. 109 (2009) 5755–5798.
[39] G.-W. Wang, Chem. Soc. Rev. 42 (2013) 7668–7700.
[40] P. Baláž, M. Achimovičová, M. Baláž, P. Billik, Z. Cherkezova-Zheleva, J.M. Criado, F. Delogu, E. Dutková, E. Gaffet, F.J. Gotor, Chem. Soc. Rev. 42 (2013) 7571–7637.
[41] D.E. Crawford, C.K. Miskimmin, A.B. Albadarin, G. Walker, S.L. James, Green Chem. 19 (2017) 1507–1518.
[42] J. Andersen, J. Mack, Green Chem. 20 (2018) 1435–1443.
[43] S.Z. Rogovina, T.A. Akopova, G.A. Vikhoreva, J. Appl. Polym. Sci. 70 (1998) 927–933.
[44] A.N. Zelenetskii, T.A. Akopova, N.R. Kildeeva, G.A. Vikhoreva, E.S. Obolonkova, A.A. Zharov, Russ. Chem. Bull. 52 (2003) 2073–2077.
[45] S.Z. Rogovina, G.A. Vikhoreva, T.Y.A. Akopova, I.N. Gorbacheva, S.N. Zelenetskii, Mendeleev Commun. 8 (1998) 107–109.
[46] T.S. Demina, T.A. Akopova, L.V. Vladimirov, A.N. Shchegolikhin, A.S. Kechek'yan, N.S. Perov, A.O. Chernyshenko, A.N. Zelenetskii, Polym. Sci. Ser. B 53 (2011) 358–370.
[47] S.Z. Rogovina, T.A. Akopova, G.A. Vikhoreva, I.N. Gorbacheva, Polym. Degrad. Stabil. 73 (2001) 557–560.
[48] T.A. Akopova, L.V. Vladimirov, V.A. Zhorin, A.N. Zelenetskii, Polym. Sci. Ser. B 51 (2009) 124–134.
[49] L.V. Lesnyakova, T.A. Akopova, G.A. Vikhoreva, A.N. Zelenetskii, L.S. Gal′Braikh, Fibre Chem. 44 (2012) 149–152.
[50] T.S. Demina, T.A. Akopova, L.V. Vladimirov, A.N. Zelenetskii, E.A. Markvicheva, C. Grandfils, Mat. Sci. Eng. C-mater 59 (2016) 333–338.
[51] T.S. Demina, K.N. Bardakova, N.V. Minaev, E.A. Svidchenko, A.V. Istomin, G.P. Goncharuk, L.V. Vladimirov, A.V. Grachev, A.N. Zelenetskii, P.S. Timashev, T.A. Akopova, Polymers 9 (2017) 302.
[52] T.A. Akopova, T.S. Demina, G.V. Cherkaev, M.A. Khavpachev, K.N. Bardakova, A.V. Grachev, L.V. Vladimirov, A.N. Zelenetskii, P.S. Timashev, RSC Adv. 9 (2019) 20968–20975.
[53] P. Du, K. Huang, X. Fan, J. Ma, N. Hussain, R. Wang, B. Deng, B. Ge, H. Tang, R. Zhang, M. Lei, H. Wu, Nano Res. 15 (2022) 3065–3072.
[54] D. Wei, T. Lindfors, C. Kvarnström, L. Kronberg, R. Sjöholm, A. Ivaska, J. Electroanal. Chem. 575 (2005) 19–26.
[55] D. Wei, C. Kvarnström, T. Lindfors, L. Kronberg, R. Sjöholm, A. Ivaska, Synth. Met. 156 (2006) 541–548.
[56] A. Petr, D. Wei, C. Kvarnström, A. Ivaska, L. Dunsch, J. Phys. Chem. B 111 (2007) 12395–12398.
[57] G. Cravotto, P. Cintas, Angew. Chem. Int. Ed. 49 (2010) 6028–6030.
[58] A. Piermattei, S. Karthikeyan, R.P. Sijbesma, Nat. Chem. 1 (2009) 133–137.
[59] B. Lee, Z. Niu, S.L. Craig, Angew. Chem. Int. Ed. 55 (2016) 13086–13089.
[60] H. Zhang, A.Z. Zoubi, M.N. Silberstein, C.E. Diesendruck, Angew. Chem. Int. Ed. 62 (2023) e202314781.
[61] A.N. Sokolov, D.K. Bucar, J. Baltrusaitis, S.X. Gu, L.R. Macgillivray, Angew. Chem., Int. Ed. Engl. 49 (2010) 4273–4277.
[62] I.N. Egorov, S. Santra, D.S. Kopchuk, I.S. Kovalev, G.V. Zyryanov, A. Majee, B.C. Ranu, V.L. Rusinov, O.N. Chupakhin, Green Chem. 22 (2020) 302–315.
[63] Q. Meng, Y. Feng, S. Han, F. Yang, M. Demiral, F. Meng, S. Araby, J. Appl. Polym. Sci. 140 (2023) e53681.
[64] A.K. Giri, J. Appl. Phys. 81 (1997) 1348–1350.
[65] L. Fang, Y. Leng, P. Gao, Biomaterials 27 (2006) 3701–3707.
[66] H.C. Huang, S.P. Huang, T.E. Hsieh, C.H. Chen, J. Appl. Polym. Sci. 123 (2012) 3199–3207.
[67] S. Deng, J. Zhang, L. Ye, Compos. Sci. Technol. 69 (2009) 2497–2505.
[68] N. Ohn, J. Shin, S.S. Kim, J.G. Kim, ChemSusChem 10 (2017) 3529–3533.
[69] G.A. Bowmaker, Chem. Commun. 49 (2013) 334–348.
[70] C. Schumacher, K.-N. Truong, J.S. Ward, R. Puttreddy, A. Rajala, E. Lassila, C. Bolm, K. Rissanen, Org. Chem. Front. 11 (2024) 781–795.
[71] Q. Liu, Y. Xu, Y. Zhao, K. Wang, C. Liang, S. Zhao, X. Wang, X. Guo, N. Xue, W. Ding, Adv. Mater. Tech. 8 (2023) 2202007.
[72] T.E. Fischer, Annu. Rev. Mater. Res. 18 (1988) 303–323.
[73] H. Carlton, D. Huitink, H. Liang, Lubricants 8 (2020) 87.
[74] V.B. Vladimir, Russ. Chem. Rev. 75 (2006) 177.
[75] S.-H. Choa, K.C. Ludema, G.E. Potter, B.M. Dekoven, T.A. Morgan, K.K. Kar, Wear 177 (1994) 33–45.
[76] J.M. Georges, J.M. Martin, T. Mathia, P. Kapsa, G. Meille, H. Montes, Wear 53 (1979) 9–34.
[77] L. Taylor, A. Dratva, H.A. Spikes, Tribol. Trans. 43 (2000) 469–479.
[78] Y. Yamamoto, S. Gondo, Tribol. Trans. 32 (1989) 251–257.
[79] C. Yan, R. Peter, L. Hong, Friction 11 (2023) 489–512.
[80] M.L.S. Fuller, M. Kasrai, G.M. Bancroft, K. Fyfe, K.H. Tan, Tribol. Trans. 31 (1998) 627–644.
[81] G.M. Bancroft, M. Kasrai, M. Fuller, Z. Yin, K. Fyfe, K.H. Tan, Tribol. Lett. 3 (1997) 47–51.
[82] M. Aktary, M.T. Mcdermott, G.A. Mcalpine, Tribol. Lett. 12 (2002) 155–162.
[83] P.C.H. Mitchell, Wear 100 (1984) 281–300.
[84] J. Graham, H. Spikes, S. Korcek, Tribol. Trans. 44 (2001) 626–636.
[85] C. Grossiord, K. Varlot, J.M. Martin, T.L. Mogne, C. Esnouf, K. Inoue, Tribol. Int. 31 (1998) 737–743.
[86] C. Grossiord, J.M. Martin, T.L. Mogne, T. Palermo, Surf. Coat. Technol. 108–109 (1998) 352–359.
[87] T. Onodera, Y. Morita, A. Suzuki, R. Sahnoun, M. Koyama, H. Tsuboi, N. Hatakeyama, A. Endou, H. Takaba, C.A. del Carpio, M. Kubo, T. Shin-Yoshi, N. Nishino, A. Suzuki, A. Miyamoto, Tribol. Online 3 (2008) 80–85.
[88] P.A. Romero, L. Mayrhofer, P. Stoyanov, R. Merz, M. Kopnarski, M. Dienwiebel, M. Moseler, Front. Mech. Eng. 5 (2019) 2297–3079.
[89] P.A. Romero, L. Mayrhofer, P. Stoyanov, R. Merz, M. Kopnarski, M. Dienwiebel, M. Moseler, Front. Mech. Eng. 5 (2019) 6.
[90] M. Qu, Y. Yao, J. He, X. Ma, S. Liu, J. Feng, L. Hou, Tribol. Int. 104 (2016) 166–174.
[91] D. Wei, A. Ivaska, Anal. Chim. Acta 607 (2008) 126–135.
[92] M. Taher, F.U. Shah, A. Filippov, P. de Baets, S. Glavatskih, O.N. Antzutkin, RSC Adv. 4 (2014) 30617–30623.
[93] Z. Li, T. Ren, Tribol. Int. 109 (2016) 373–381.
[94] S. Arrhenius, Z. Phys. Chem. 4U (1889) 96–116.
[95] F.P. Bowden, M.A. Stone, G.K. Tudor, A.C.D. Rivett, R. Robertson, Proc. Roy. Soc. Lond. A 188 (1947) 329–349.
[96] T. Sakurai, K. Sato, A S L E Transactions 9 (1966) 77–87.
[97] K. Nakayama, J. Martin, Wear 26 (2006) 235–240.
[98] S. Mori, T. Kawada, W.-C. Xu, Appl. Surf. Sci. 108 (1997) 391–397.
[99] C. Kajdas, K. Hiratsuka, Proc. Inst. Mech. Eng. Part J, J. Eng. Tribol. 223 (2009) 827–848.

[100] P. Li, J. Wu, Z. Wu, Y. Jia, J. Ma, W. Chen, L. Zhang, J. Yang, Y. Liu, Nano Energy 63 (2019) 103832.
[101] J. Zhao, L. Chen, W. Luo, H. Li, Z. Wu, Z. Xu, Y. Zhang, H. Zhang, G. Yuan, J. Gao, Ceram. Int. 46 (2020) 25293–25298.
[102] K.-S. Hong, H. Xu, H. Konishi, X. Li, J. Phys. Chem. Lett. 1 (2010) 997–1002.
[103] N. Meng, W. Liu, R. Jiang, Y. Zhang, S. Dunn, J. Wu, H. Yan, Prog. Mater. Sci. 138 (2023) 101161.
[104] T. Jiang, Y. Wang, Z. Guo, H. Luo, C. Zhan, Y. Wang, Z. Wang, F. Jiang, H. Chen, J. Clean. Prod. 341 (2022) 130908.
[105] Q. Wang, X. Guo, W.L. Shi, F. Guo, Y. Yan, X. Lin, Nanosci. Nanotechnol. Lett. 7 (2015) 691–696.
[106] Y.-L. Liu, J.M. Wu, Nano Energy 56 (2019) 74–81.
[107] W. Qian, K. Zhao, D. Zhang, C.R. Bowen, Y. Wang, Y. Yang, ACS Appl. Mater. Interfaces 11 (2019) 27862–27869.
[108] Y. Du, T. Lu, X. Li, Y. Liu, W. Sun, S. Zhang, Z. Cheng, Nano Energy 104 (2022) 107919.
[109] K. Wang, C. Han, J. Li, J. Qiu, J. Sunarso, S. Liu, Angew. Chem. Int. Ed. 61 (2022) e202110429.
[110] Y. Wang, X. Wen, Y. Jia, M. Huang, F. Wang, X. Zhang, Y. Bai, G. Yuan, Y. Wang, Nat. Commun. 11 (2020) 1328.
[111] X. Chen, Y. Li, X. Pan, D. Cortie, X. Huang, Z. Yi, Nat. Commun. 7 (2016) 12273.
[112] Y. Lu, W.-J. Yin, K.-L. Peng, K. Wang, Q. Hu, A. Selloni, F.-R. Chen, L.-M. Liu, M.-L. Sui, Nat. Commun. 9 (2018) 2752.
[113] W. Tong, Y. Zhang, H. Huang, K. Xiao, S. Yu, Y. Zhou, L. Liu, H. Li, L. Liu, T. Huang, M. Li, Q. Zhang, R. Du, Q. An, Nano Energy 53 (2018) 513–523.
[114] X. Yan, G. Li, Z. Wang, Z. Yu, K. Wang, Y. Wu, Nano Energy 77 (2020) 105180.
[115] X. Jia, H. Wang, H. Lei, C. Mao, X. Cui, Y. Liu, Y. Jia, W. Yao, W. Chen, J. Adv. Ceram. 12 (2023) 2271–2283.
[116] Z. Liang, C.-F. Yan, S. Rtimi, J. Bandara, Appl. Catal., B 241 (2019) 256–269.
[117] S. Singh, N. Khare, Nano Energy 38 (2017) 335–341.
[118] S. Masimukku, Y.-C. Hu, Z.-H. Lin, S.-W. Chan, T.-M. Chou, J.M. Wu, Nano Energy 46 (2018) 338–346.
[119] K. Kubota, Y. Pang, A. Miura, H. Ito, Science 366 (2019) 1500–1504.
[120] F. Meng, W. Ma, C. Duan, X. Liu, Z. Chen, M. Wang, J. Gao, Z. Zhang, Appl. Catal., B 252 (2019) 187–197.
[121] F. Meng, W. Ma, Y. Wang, Z. Zhu, Z. Chen, G. Lu, Environ. Sci.: Nano (2020) 1704–1718.
[122] T.Y. Zhang, C.F. Gao, Theor. Appl. Fract. Mech. 41 (2004) 339–379.
[123] S.S. Anandakrishnan, M. Tabeshfar, M. Nelo, J. Peräntie, H. Jantunen, J. Juuti, Y. Bai, RSC Sustain. 2 (2024) 961–974.
[124] S. Xu, W. Qian, D. Zhang, X. Zhao, X. Zhang, C. Li, C.R. Bowen, Y. Yang, Nano Energy 77 (2020) 105305.
[125] B. Chen, Y. Xia, R. He, H. Sang, W. Zhang, J. Li, L. Chen, P. Wang, S. Guo, Y. Yin, L. Hu, M. Song, Y. Liang, Y. Wang, G. Jiang, R.N. Zare, Proc. Natl. Acad. Sci. U.S.A. 119 (2022) e2209056119.
[126] J. Zhang, M.L. Coote, S. Ciampi, J. Am. Chem. Soc. 143 (2021) 3019–3032.
[127] J. Nie, Z. Ren, L. Xu, S. Lin, F. Zhan, X. Chen, Z.L. Wang, Adv. Mater. 32 (2020) e1905696.
[128] S. Lin, L. Xu, A. Chi Wang, Z.L. Wang, Nat. Commun. 11 (2020) 399.
[129] J. Zhang, S. Lin, Z.L. Wang, ACS Nano 17 (2023) 1646–1652.
[130] Z. Wang, A. Berbille, Y. Feng, S. Li, L. Zhu, W. Tang, Z.L. Wang, Nat. Commun. 13 (2022) 130.
[131] X. Dong, Z. Wang, A. Berbille, X. Zhao, W. Tang, Z.L. Wang, Nano Energy 99 (2022) 107346.
[132] X. Zhao, Y. Su, A. Berbille, Z.L. Wang, W. Tang, Nanoscale 15 (2023) 6243–6251.
[133] C.-Y. Liu, A.J. Bard, Chem. Phys. Lett. 485 (2010) 231–234.
[134] C. Liu, A.J. Bard, Nat. Mater. 7 (2008) 505–509.
[135] C.Y. Liu, A.J. Bard, J. Am. Chem. Soc. 131 (2009) 6397–6401.
[136] J. Zhang, F.J.M. Rogers, N. Darwish, V.R. Gonçales, Y.B. Vogel, F. Wang, J.J. Gooding, M.C.R. Peiris, G. Jia, J.-P. Veder, M.L. Coote, S. Ciampi, J. Am. Chem. Soc. 141 (2019) 5863–5870.
[137] S. Piperno, H. Cohen, T. Bendikov, M. Lahav, I. Lubomirsky, Angew. Chem. Int. Ed. 50 (2011) 5654–5657.
[138] M.W. Williams, AIP Adv. 2 (2012) 010701.
[139] B. Baytekin, H.T. Baytekin, B.A. Grzybowski, J. Am. Chem. Soc 134 (2012) 7223–7226.
[140] D.J. Lacks, R. Mohan Sankaran, J. Phys. D Appl. Phys. 44 (2011) 453001.
[141] C. Yun, S.-H. Lee, J. Ryu, K. Park, J.-W. Jang, J. Kwak, S. Hwang, J. Am. Chem. Soc. 140 (2018) 14687–14695.
[142] B.D. Gates, Q. Xu, M. Stewart, D. Ryan, C.G. Willson, G.M. Whitesides, Chem. Rev. 105 (2005) 1171–1196.
[143] H.T. Baytekin, B. Baytekin, T.M. Hermans, B. Kowalczyk, B.A. Grzybowski, Science 341 (2013) 1368–1371.
[144] S. Lin, X. Chen, Z.L. Wang, Chem. Rev. 122 (2022) 5209–5232.
[145] S. Lin, L. Xu, A. Chi Wang, Z.L. Wang, Nat. Commun. 11 (2020) 399.
[146] Z. Wang, X. Dong, W. Tang, Z.L. Wang, Chem. Soc. Rev. 53 (2024) 4349–4373.
[147] J. Zhang, S. Lin, M. Zheng, Z.L. Wang, ACS Nano 15 (2021) 14830–14837.
[148] J. Zhang, S. Lin, Z.L. Wang, J. Phys. Chem. B 126 (2022) 2754–2760.
[149] Z. Wang, A. Berbille, Y. Feng, S. Li, L. Zhu, W. Tang, Z.L. Wang, Nat. Commun. 13 (2022) 130.
[150] M. Hayyan, M.A. Hashim, I.M. Alnashef, Chem. Rev. 116 (2016) 3029–3085.
[151] H. Li, A. Berbille, X. Zhao, Z. Wang, W. Tang, Z.L. Wang, Nat. Energy 8 (2023) 1137–1144.
[152] J. Zhao, X. Zhang, J. Xu, W. Tang, Z. Lin Wang, F. Ru Fan, Angew. Chem. Int. Ed. 62 (2023) e202300604.
[153] W. Li, J. Sun, M. Wang, J. Xu, Y. Wang, L. Yang, R. Yan, H. He, S. Wang, W.-Q. Deng, Z.-Q. Tian, F.R. Fan, Angew. Chem. Int. Ed. 63 (2024) e202403114.
[154] Y. Su, A. Berbille, X.-F. Li, J. Zhang, M. PourhosseiniAsl, H. Li, Z. Liu, S. Li, J. Liu, L. Zhu, Z.L. Wang, Nat. Commun. 15 (2024) 4196.
[155] Z. Wang, X. Dong, X.-F. Li, Y. Feng, S. Li, W. Tang, Z.L. Wang, Nat. Commun. 15 (2024) 757.
[156] Y. Zhao, Y. Liu, Y. Wang, S. Li, Y. Liu, Z.L. Wang, P. Jiang, Nano Energy 112 (2023) 108464.
[157] M. Zhang, W.-Z. Song, T. Chen, D.-J. Sun, D.-S. Zhang, C.-L. Li, R. Li, J. Zhang, S. Ramakrishna, Y.-Z. Long, Nano Energy 110 (2023) 108329.
[158] S. Li, Z. Zhang, P. Peng, X. Li, Z.L. Wang, D. Wei, Nano Energy 122 (2024) 109286.
[159] B. Jiang, X. Xue, Z. Mu, H. Zhang, F. Li, K. Liu, W. Wang, Y. Zhang, We. Li, C. Yang, K. Zhang, Molecules (27) (2022) 8579.
[160] C. Wang, R. Zhao, W. Fan, L. Li, H. Feng, Z. Li, C. Yan, X. Shao, K. Matyjaszewski, Z. Wang, Angew. Chem. Int. Ed. 62 (2023) e202309440.

Dr. Shaoxin Li is a post-doctor in the Beijing Institute of Nanoenergy and Nanosystems. She achieved the Ph.D degree from the University of Chinese Academy of Sciences in 2022 and the B.S. degree from the Jiangsu University in 2017. Her research interest is self-powered sensors, energy harvesting, and solid–liquid contact electrification.

Jiajin Liu achieved his B. E. degree from the Jilin University in 2021. He is studying for a M. S. degree at the Beijing Institute of Nanoenergy and Nanosystems. His research interest is solid–liquid electrification and contact-electro chemistry.

Prof. Zhong Lin Wang received his Ph.D. from Arizona State University in physics. He now is the Hightower Chair in Materials Science and Engineering, Regents' Professor, Engineering Distinguished Professor and Director, Center for Nanostructure Characterization, at Georgia Tech. Dr. Wang has made original and innovative contributions to the synthesis, discovery, characterization and understanding of fundamental physical properties of oxide nanobelts and nanowires, as well as applications of nanowires in energy sciences, electronics, optoelectronics and biological science. His discovery and breakthroughs in developing nanogenerators established the principle and technological road map for harvesting mechanical energy from environment and biological systems for powering personal electronics. His research on self-powered nanosystems has inspired the worldwide effort in academia and industry for studying energy for micro-nano-systems, which is now a distinct disciplinary in energy research and future sensor networks. He coined and pioneered the field of piezotronics and piezophototronics by introducing piezoelectric potential gated charge transport process in fabricating new electronic and optoelectronic devices. Details can be found at: http://www.nanoscience.gatech.edu.

Prof. Di Wei serves as the Principal Investigator at BINN and heads the Iontronics Laboratory. As Fellow of National Academy of Inventors (FNAI) USA, Fellow of the Royal Society of Chemistry (FRSC) UK, Fellow of Institute of Materials, Minerals & Mining (FIMMM) UK and Senior Member of Wolfson College at Cambridge University, he has published over 120 papers including Nat. Energy, Nat. Commun., Sci. Adv., PNAS, Joule, Matter, Adv. Mater., Angew. Chem. Int. Ed., J. Am. Chem. Soc., Energ. Environ. Sci., Chem. Soc. Rev. etc. as the first/corresponding author. Prof. Wei also has a portfolio of over 200 international patents (including PCT). Notably, over 100 patents have been successfully granted, many of which have been transferred to leading companies like Nokia in Finland and Lyten in the USA. Additionally, Prof. Wei has edited 6 English books, published by Wiley and Cambridge University Press etc., focusing on nanotechnology for energy and information technology. His achievements have been recognized by the first prize of the Nokia Global Innovation and Excellence Award, Brian Conway Prize in Physical Electrochemistry from the International Society of Electrochemistry (ISE) and various other prizes from ISE and RSC. Details can be found at: http://www.iontronics.group/en/.